catalysts

MDPI

Review

Nanomaterials for Photocatalytic Degradations of Analgesic, Mucolytic and Anti-Biotic/Viral/Inflammatory Drugs Widely Used in Controlling SARS-CoV-2

Mahsa Ebrahimi and Omid Akhavan *

Department of Physics, Sharif University of Technology, P.O. Box 11155-9161 Tehran, Iran; mahsa.e.1378@gmail.com

* Correspondence: oakhavan@sharif.edu; Tel.: +98-21-66164566; Fax: +98-21-66022711

Abstract: The COVID-19 pandemic has been transformed into one of the main worldwide challenges, in recent years. For controlling symptoms that are caused by this disease (e.g., chills or fever, shortness of breath and/or difficulty in breathing, cough, sore throat, fatigue, headache, muscle aches, the new loss of tastes and/or smells, congestion or runny nose, nausea, vomiting and/or diarrhea), lots of medicines including analgesics, mucolytics, and anti-biotic/viral/inflammatory drugs have been frequently prescribed. As these medicines finally contaminate terrestrial and aquatic habitats by entering surface waterways through pharmaceutical production and excreting trace amounts of waste after human usage, they have negative impacts on wildlife's health and ecosystem. Residual drugs in water have the potential to harm aquatic creatures and disrupt their food chain as well as the breeding cycle. Therefore, proper degradation of these broadly used medicines is highly crucial. In this work, the use of nanomaterials applicable in photocatalytic degradations of analgesics (e.g., acetaminophen, aspirin, ibuprofen, and naproxen), mucolytics (e.g., ambroxol), antibiotics (e.g., azithromycin and quinolones including hydroxychloroquine and chloroquine phosphate), anti-inflammatory glucocorticoids (e.g., dexamethasone and cortisone acetate), antihistamines (e.g., diphenhydramine), H2 blockers (e.g., famotidine), anthelmintics (e.g., praziquantel), and finally antivirals (e.g., ivermectin, acyclovir, lopinavir/ritonavir, favipiravir, nitazoxanide, and remdesivir) which widely used in controlling/treating the coronavirus have been reviewed and discussed.

Keywords: nanomaterials; catalysts; pharmaceutical wastes; antibiotics; antiviral drugs; COVID-19

check for updates

Citation: Ebrahimi, M.; Akhavan, O. Nanomaterials for Photocatalytic Degradations of Analgesic, Mucolytic and Anti-Biotic/Viral/Inflammatory Drugs Widely Used in Controlling SARS-CoV-2. *Catalysts* **2022**, *12*, 667. https://doi.org/10.3390/catal12060667

Academic Editors: Elhassan Amaterz, Zakaria Anfar, Abdallah Amedlous and Abdessalam Bouddouch

Received: 12 May 2022
Accepted: 15 June 2022
Published: 18 June 2022

Publisher's Note: MDPI stays neutral with regard to jurisdictional claims in published maps and institutional affiliations.

Copyright: © 2022 by the authors. Licensee MDPI, Basel, Switzerland. This article is an open access article distributed under the terms and conditions of the Creative Commons Attribution (CC BY) license (https://creativecommons.org/licenses/by/4.0/).

1. Introduction

As a new challenge, the SARS-CoV-2 virus results in the COVID-19 pandemic. Based on WHO reports, there have been ~250 million cases of COVID-19 confirmed by PCR-based tests, including ~5 million deaths till now, in spite of the huge consumption of medicines with probable effects. Sneezing, coughing, face-to-face chatting, and any unhealthy activity can result in the transmission of the virus. Droplets that contain viruses are discharged into the air or attached to surfaces through these actions. Other people could be infected with the virus by inhaling the droplets or receiving them in their mouth, nose, or eyes. Hence, control and treatment of COVID-19 have become a worldwide challenge for humankind, countries, and governments. Based on the mechanism of action, some drugs have been broadly prescribed to combat symptoms of COVID-19. For example, at the first stage of the disease, COVID-19 patients usually suffer from muscle pain, headache, eye pain, abdominal pain, and general aches. Therefore, there is a vital need for some drugs which can relieve the pain. Based on this information, painkillers became popular and have been widely used among patients. Two categories of analgesics are anti-inflammatory medicines, which relieve pain by decreasing local inflammatory reactions (inhibition of cyclooxygenase, the enzyme responsible for the production of prostaglandins), and opioids, which operate on the brain (Activation of descending inhibitory controls in the midbrain and suppression of

neurotransmitter release from primary afferent terminals in the spinal cord [1]). Meanwhile, for control of coughing in patients, mucolytic drugs are most effective that are commonly used to treat respiratory problems, because they can dissolve thick mucus by breaking molecular connections that hold the mucus molecules together [2]. In the next step, doctors may give antibiotics to patients to prevent/control bacterial infections, even though all of us know that antibiotics cannot treat COVID-19 as a disease caused by a virus. The basic mechanisms relating to the action of antibiotics include: (1) cell wall synthesis inhibition (as the most common mechanism), (2) protein synthesis inhibition (as the second largest class), (3) nucleic acid synthesis inhibition, (4) cell membrane alteration, and (5) antimetabolite activity [3,4]. However, in some severe cases of coronavirus infections, severe inflammation and ARDS-related lung injury may lead to alveolar damage. In such cases, corticosteroid medications such as anti-inflammatory drugs have been administered to reduce immune-mediated lung tissue destruction. However, the action mechanisms of these drugs depend on their concentrations. For example, dexamethasone's mechanism of action is strongly dependent on its dosage: (1) the genomic mechanism (in low doses) and (2) the non-genomic mechanisms (in high doses). The genomic mechanism is more effective, but it needs a long period and high consumption, and probably a high waste of the drug. Furthermore, even though the effect of non-genomic mechanisms may occur rapidly, it can induce a higher risk of side effects [5]. It is interesting to note that among antihistamines, diphenhydramine, hydroxyzine, and azelastine have shown antiviral effects against coronavirus [6]. Nevertheless, the mechanisms through which antihistamines produce antiviral effects are unknown [7]. H2 blockers may help to control gastrointestinal symptoms of COVID-19, such as diarrhea, vomiting, or belly pain. H2RAs reduce stomach acid output by binding to histamine H2 receptors on gastric oxyntic cells reversibly, reducing the endogenous ligand histamine's activity and binding [8]. Antiviral medicines including lopinavir/ritonavir, nelfinavir, perampanel, pitavastatin, and praziquantel are also used for the treatment of COVID-19. Antiviral drugs can enhance the resistibility of cells against viruses such as decreasing the virus's adsorption, diffusion, and deproteinization processes in the cell (amantadine) along with antimetabolites that inhibit the production of nucleic acids [9].

This wide usage of drugs against coronavirus will certainly pollute our environment and finally cause lots of damage to the ecosystem. Surface waterways may eventually be contaminated by residues produced during usage, excretion, or clinical waste disposal procedures. For example, the concentration of azithromycin in surface water significantly increased from 4.3 ng L^{-1} (before the COVID-19 pandemic) [10] to 935 ng L^{-1} (after the pandemic) [11,12]. Meantime, significant amounts of human medications can excrete into the sewage system after ingestion, without effective absorption and/or chemical processing [13]. These can lead to further and faster formation of antibiotic-resistant bacteria in the near future as a new certain challenge for the international community [14]. In addition, the high and frequent use of antiviral drugs in a short time for controlling SARS-CoV-2 can result in resistance to the antivirals, as another important challenge [15]. Based on a report, the concentrations of antiviral medications showed a ~70% rise in urban wastewaters during the pandemic, as compared to the concentrations monitored before the pandemic [16]. Therefore, in addition to substituting the conventional drug therapy with green methods (such as the application of active nanobubbles in the treatment of hypoxic COVID-19 patients [17]), finding proper environment-friendly degradation methods for removing these huge amounts of used drugs is highly important, because the pharmaceutical wastes can be transformed into a new challenge for human, our health and environment, in the near future.

Nanotechnology-based photocatalysis is known as a green technology that has emerged as a viable option for degrading/removing/treating a variety of organic/inorganic contaminants, risks, and hazards such as industrial wastes [18], dye molecules [19], pesticides [20], poisons [21], crude oil stains [22], polyaromatic hydrocarbons [23], cancerous cells [24], bacteria [25], bacteria resistant to antibiotics [26], molds [27], viruses [28,29], parasitic organisms [30], and pharmaceutical wastes [31]. Semiconductors are always present in these

compounds because of their potential uses in the conversion of solar energy [32–34]. Several semiconductors (such as TiO_2 [35], ZnO [36], Fe_2O_3 [37], SnO_2 [38], CuO [39], CeO_2 [40], CdS [41], ZnS [42], and others [43]) have been investigated as effective photocatalysts, but TiO_2-based nanomaterials have received the most attention due to their capacity to degrade organic contaminants, accomplish full mineralization [44], and capability of efficient working under solar light irradiation [45,46]. In addition, TiO_2 is one of the most efficient photocatalyst resistant to many chemicals with essentially non-toxic, cheap, plentiful, and water-insoluble/dispersible characteristics [47]. It possesses three crystalline phase formations: anatase, rutile, and brookite. Anatase phase shows stronger photocatalytic activity than rutile in pure phases of TiO_2. In this regard, recent degradations of pharmaceutical wastes by using photocatalytic nanoparticles (NPs), especially TiO_2 NPs, have drawn much attention [48–51].

The high mortality rate due to corona in many countries caused simultaneous extensive usage of analgesic, mucolytic and anti-biotic/viral/inflammatory drugs by many peoples (whether suspected or definitively infected), resulting in obvious higher consumption/distribution of the drugs (either in hospitals or by ordinary peoples) and so unwanted contamination of the living environment and surface water [12]. Therefore, suitable management of the widely used pharmaceutical wastes is an important task [15]. However, limited research/review reports relating to photocatalytic degradations of pharmaceutical wastes produced during the control of the SARS-CoV-2 virus have been reported so far. This review aimed to highlight that proper management of the pharmaceutical wastes produced during COVID-19 is urgent and there are some photocatalytic-based methods for decreasing their potential side effects. Since the drugs are synthesized based on organic chemistry, the byproducts of the photocatalytic degradation are mainly CO_2 and H_2O, although some NO_x, SO_x, Cl, F, Br, and/or P residuals are inevitably expected, depending on the basic chemical composition of the drug. In this regard, the application of suitable nanomaterials in photocatalytic degradations of the various drugs broadly utilized in treating/controlling the corona pandemic has been reviewed. The degradations of drugs considered/discussed in this study are analgesics (including acetaminophen, aspirin, ibuprofen, and naproxen), mucolytics (including ambroxol), antibiotics (e.g., azithromycin and quinolones including hydroxychloroquine and chloroquine phosphate), anti-inflammatory glucocorticoids (including dexamethasone and cortisone acetate), antihistamines (such as diphenhydramine), H2 blockers (e.g., famotidine), anthelmintics (e.g., praziquantel), and more importantly antivirals (including ivermectin, acyclovir, lopinavir/ritonavir, favipiravir, nitazoxanide, and remdesivir). This review can draw more attention to human health, by further introducing the green methods providing effective controlling/disposing of the pharmaceutical wastes in our environment.

2. Analgesics

Analgesics, often known as painkillers, are medicines that alleviate a variety of pains, including headaches, injuries, and arthritis. Anti-inflammatory analgesics decrease inflammation, whereas opioid analgesics alter pain perception in the brain [52,53].

2.1. Acetaminophen

Paracetamol (also known as acetaminophen (ACT) and paracetamol, IUPAC name: N-(4-hydroxyphenyl)acetamide, N-(4-hydroxyphenyl)ethanamide, molecular formula: $C_8H_9NO_2$) is a fever reducer that can also assist with the muscular discomfort and body pains caused by COVID-19. ACT does not treat the infection and does not shorten the length of your sickness. Acetaminophen and structural analogs are widely distributed in nature and quickly concentrate in the aquatic environment, where they have been found all over the world in surface waters, sewage, and drinking water [54]. ACT was identified as one of 95 wastewater pollutants in 139 U.S. streams by a National Reconnaissance conducted in 1999–2000. Also, non-prescription medications were discovered in 81% of the

streams examined with concentrations as high as 10 ppb [55]. In this part of the paper, we will review one of the solutions to this problem: photocatalytic degradation of ACT.

In an investigation, Dalida et al. [56] looked at how acetaminophen (ACT) was broken down photocatalytically in a synthetic titanium dioxide (TiO_2, anatase phase) solution, under visible light irradiation ($\lambda > 440$ nm). The $KAl(SO_4)_2$ and $NaAlO_2$ doped TiO_2 photocatalyst were produced using the sol–gel technique. Initial pH, the dosage of the photocatalyst, and the initial concentration of ACT were all investigated as potential influences on acetaminophen breakdown. It was also established what the best operating conditions were. The results revealed that synthesized TiO_2 catalysts primarily displayed an anatase phase with no rutile phase. LED alone broke down negligible quantities of ACT, according to the photocatalytic degradation data, but when $TiO_2/KAl(SO_4)_2$ was present, 95% elimination of 0.10-mM ACT was accomplished in 540 min of the time of irradiation. The photocatalytic degradation of acetaminophen by synthetic $TiO_2/KAl(SO_4)_2$ was superior to Degussa P-25, which is commercially available. The photocatalytic degradation of $TiO_2/NaAlO_2$ photocatalyst was lower than $TiO_2/KAl(SO_4)_2$ due to the poor crystallinity of the photocatalyst. At 30 °C and pH 6.9, the optimum operating conditions were reached by using a dosage of 1.0 g/L$TiO_2/KAl(SO_4)_2$. The pseudo-first-order model matches the photocatalytic breakdown of acetaminophen effectively, according to a kinetic investigation. The degradation rate of ACT was influenced by competitive reactions from intermediates, which became more apparent as the original ACT concentration rose.

In a recent investigation [57], high-performance liquid chromatography (HPLC), UV spectroscopy, and measurement of the zeta potential in relation to the pH of the solution were used to investigate the photodegradation of paracetamol using TiO_2 nanotubes (crystal structure of 80% anatase and 20% rutile) at a wavelength of light of 254 nm. After 100 min of exposure, the paracetamol (20 mg L^{-1}) photodegradation was 99% effective. The rate constant might be calculated by using the Langmuir–Hinshelwood equation. Under the circumstances of the chromatographic analysis, by-products that are not organic were identified. At pH 6.5, the photoreaction was quicker, indicating that adsorption was preferred, resulting in better efficiency.

In another work [58], TiO_2 was supported on Al_2SiO_5 salvaged from discarded LED panels ($ATiO_2$, anatase phase) to examine paracetamol degradation in a batch method. The synthesized $ATiO_2$ had a spherical shape, with predomination of TiO_2 in the anatase phase and a typical size of almost 15 nm. Following that, utilizing a central composite design (CCD), the impacts of operational parameters, for example, the initial concentration of ACT (1–10 mg/L), the catalyst dose (ranging from 0.5 to 4.0 g/L), and the pH range of 4–10 on ACT breakdown were investigated. To study the linear and interaction effects of operational factors on paracetamol degradation efficiency, a polynomial model was constructed. At optimal circumstances (the $ATiO_2$ dose of 2.71 g/L, initial paracetamol concentration of 2.74 mg/L, and pH of 9.5), paracetamol degradation efficiency was about 99%. Adsorption on Al_2SiO_5 and subsequent breakdown by TiO_2 were the mechanisms for paracetamol degradation. $ATiO_2$ could be reused up to three times with just a 5% reduction in degradation efficiency. Figure 1 presents a schematic diagram of the process and results.

In another study [59], the ACT photocatalytic degradation in water was investigated by TiO_2 (anatase phase) materials that are supported by Zeolite Socony Mobil-5 (ZSM-5) produced using a sol–gel technique. The structural characteristics of the photocatalysts were studied by using SEM, XRD, and surface area measurements using Brunauer–Emmett–Teller (BET). The optimum loading amount was 40 wt% for TiO_2 over ZSM-5, and the initial concentration of ACT was kept at 15 mg L^{-1} accompanied by intensity irradiations which were as low as 0.97 mW cm^{-2}. After 180 min of irradiation, the degradation rate reached 96.6%. Ace degradation is thought to begin with hydroxylation and photolysis. The main intermediate reactions and products were examined by using the GC–MS technique. Furthermore, the material was regenerated four times, whereas ACT's deterioration persisted at a higher level of around 90%.

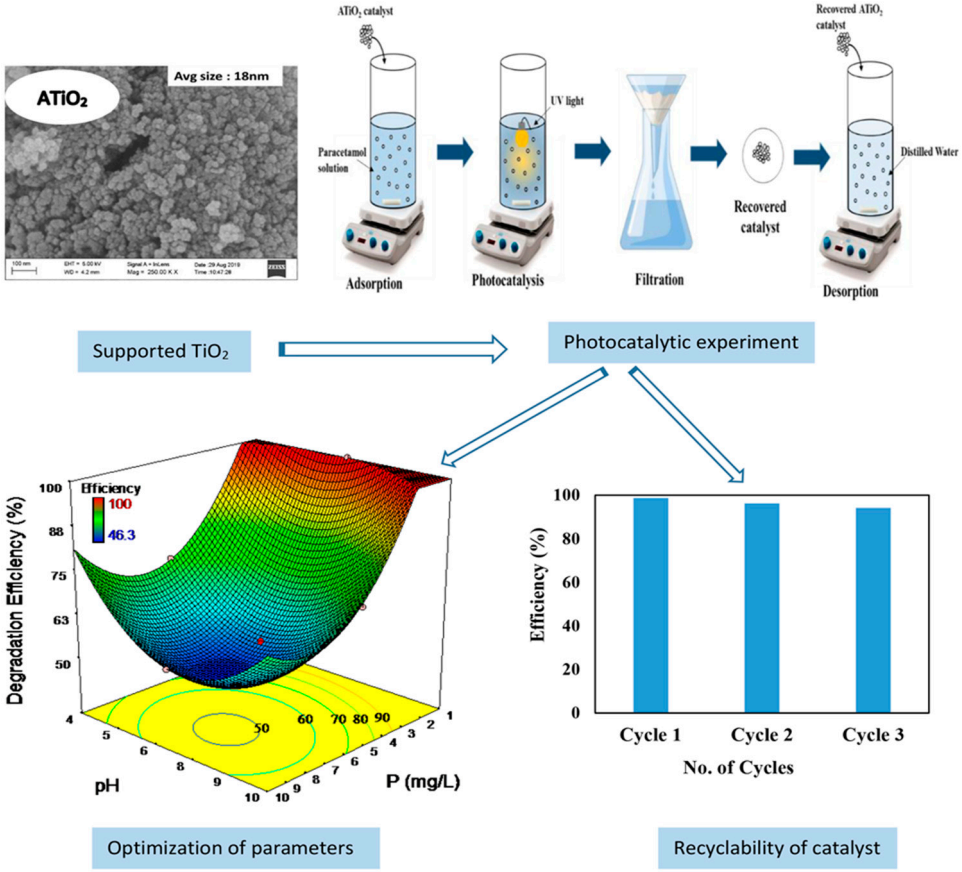

Figure 1. Photocatalytic degradation of ACT: TiO_2 is supported on aluminosilicate salvaged from discarded LED ($ATiO_2$) panels to examine ACT degradation in a batch method. $ATiO_2$ could be reused up to three times with just a 5% reduction in degrading efficiency. Reprinted/adapted with permission from Ref. [58]. Copyright 2020 IWA (Open Access).

The photocatalytic degradation of ACT in a reactor employing TiO_2 P25 (anatase 80% and rutile 20%) photocatalyst under UV light and slurry was studied by N. Jallouli et al. [60]. When paracetamol was photodegraded using TiO_2 P25 nanoparticles, it deteriorated considerably quicker and effectively, with >90% of 2.65×10^4 M ACT breaking down under UV light radiation. The adsorption and photodegradation of ACT were influenced by pH changes. The photodegradation of paracetamol is shown to be best at pH 9.0. During the ACT, HPLC discovered hydroquinone, 1,2,4-trihydroxybenzene, p-nitrophenol, and benzoquinone TiO_2-assisted photodegradation, for the first time, among them, certain pathway products are revealed. The findings indicated that the TiO_2 suspension/UV system has more efficiency for photocatalytic degradation of paracetamol in comparison to the TiO_2/cellulosic fiber mode coupled with sunlight. The TiO_2 immobilization over a slurry system has numerous advantages since it can increase adsorption characteristics while enabling simple photocatalyst separation from the treated solution, resulting in better performance that may be reused.

Magnetic nanoparticles (NPs) based on iron oxides were used in a recent study [61] to enhance their elimination by photocatalytic degradation. Apart from being inexpensive and abundant, the magnetic characteristics of these NPs make it simple to remove them from the solution once the reaction is finished. Three kinds of hematite-based NPs were synthesized and characterized: one pure (first one) and two partially consisting of a magnetite core (the second one) or entirely (the third one) coated by a hematite shell. The second sample was the most effective photocatalyst for the photo-assisted breakdown of both contaminants. Total ACT and caffeine breakdown (20 ppm/150 mL) were accomplished in 45 min and 60 min, respectively, under UV-vis irradiation and utilizing a solution of 0.13 g catalyst/L. Liquid

chromatography and electrospray ionization mass spectrometry were used to identify some of the intermediate intermediates. A supplementary Density Functional Theory (DFT) research demonstrated the relative stability of various species produced during the ACT and caffeine breakdown processes and provided some insight into the most advantageous degradation routes.

In another investigation [62], the goal was to achieve rapid photocatalytic performance by thermal oxidation etching graphite-like carbon nitride (g-C_3N_4) bulk materials to nanosheet structures. To convert the multilayer g-C_3N_4 structure to nanosheet material, a simple thermal oxidation etching process was utilized. The photocatalytic efficiency of acetaminophen and levofloxacin degradation was evaluated under direct solar irradiation. The XRD, particle size, and BET findings exhibited some fluctuation, suggesting that the etching process was developed to reduce particle size and layer number in the g-C3N4 bulk sample. The FTRI and XPS spectra indicated some changes in the g-C3N4 nanosheet motif like the CO, C-H, and N pyridinic structures, indicating some variation in optical and bandgap characteristics. As a result, the photocatalytic breakdown of acetaminophen by nanosheets of g-C3N4 under sun irradiation was considerably quicker, reaching 99% in one hour, compared to 38% in four hours for the g-C3N4 bulk sample. Likewise, levofloxacin breakdown with a sample in the form of a nanosheet got to 99% in the first hour, compared to 16% when the bulk sample was present. This improvement can be ascribed to a variety of reasons, including the g-C3N4 nanosheets' reduced particle size, decreased bandgap, and rich carbon surface. This suggests that using this technique, the performance of g-C3N4 may be improved even further and that it can be utilized to treat pharmaceutically polluted wastewater under sun irradiation.

Also to degrade ACT, Bi-modified titanate nanomaterials (Bi-TNM) come in three different morphologies and were produced using the hydrothermal technique and regulated conditions [63]. ACT is a drug with a high rate of use that is found in large quantities in wastewater and natural waters. XRD, SEM, FT-IR, UV-vis DRS, and zeta potential analyzers were used to characterize the prepared samples. Using flake, bulk, and ribbon-shaped titanate catalysts, Bi-TNM morphological effects on the photocatalytic breakdown of aqueous ACT were thoroughly studied. The influence of catalyst morphology, catalyst dose, ACT concentration, and pH of the solution on the photocatalytic activity of the prepared catalysts was evaluated. For ACT degradation, the Bi- TNM's photocatalytic activity/performance, kinetics, and mechanism were optimized. The findings reveal that the Bi-TNM photocatalyst improved visible light absorption and increased the photoinduced charge transfer efficiency, leading to great efficiency for ACT degradation. Under visible light irradiation, the photocatalytic performance of the Bi-TNM nanoribbons was considerably enhanced. The titanate nanoribbons (Bi-TNR) > the titanate nanobulks (Bi-TNB) > the titanate nanosheets (Bi-TNS) showed the greatest photocatalytic performance for ACT degradation. For the degradation of ACT, nanoribbons have a high photocatalytic activity due to their morphology. Furthermore, during the three catalytic reactions, there was no inactivation, and Bi- TNR had perfect photocatalytic stability. The photocatalytic breakdown of ACT seems to obey pseudo-first-order kinetics, under visible light based on kinetic studies. The mechanism revealed that the hole in Bi-TNR is primarily responsible for ACT photodegradation as shown in Figure 2. In comparison to pristine titanate, Bi-TNM makes a superior photocatalytic breakdown pathway for the ACT and other stubborn organic pollutants in wastewater treatment in this work.

> *One of the most frequently recommended pain relievers is non-steroidal anti-inflammatory drugs (NSAID) [64]. In soil, surface water, wastewater, groundwater, Antarctic ice, snow, sediments, and drinking water, NSAIDs have been detected in nanograms and micrograms. NSAIDs have long-term ecotoxic impacts on ecosystems, despite their low observable levels in the environment [65].*

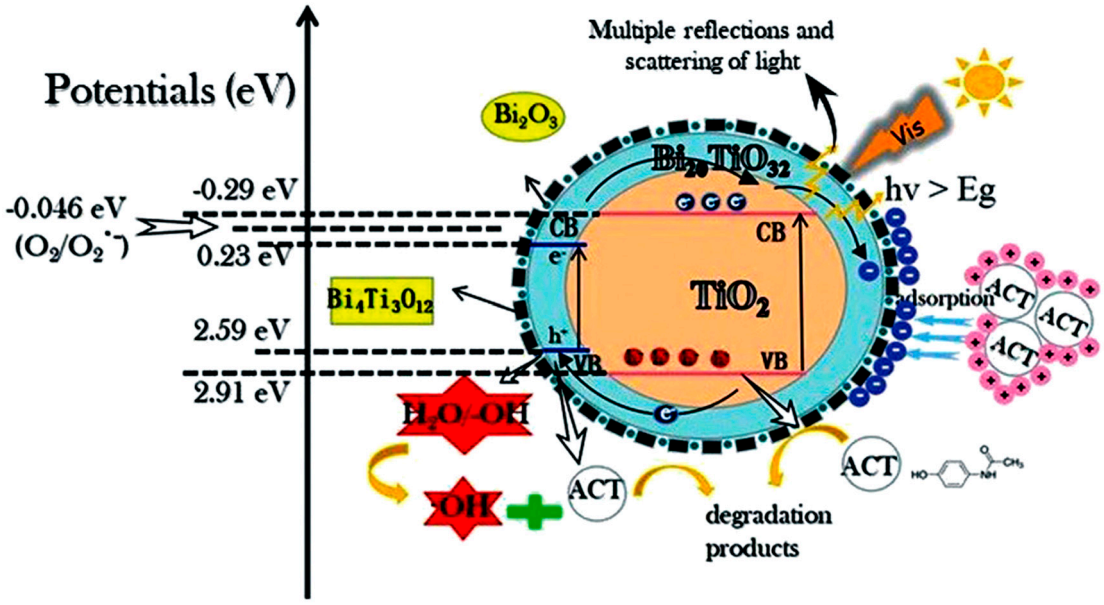

Figure 2. The proposed mechanism of ACT photocatalytic reaction by using Bi−TNR under visible light radiation. Reprinted/adapted with permission from Ref. [63]. Copyright 2018 Royal Society of Chemistry.

2.2. Aspirin

Aspirin (also known as acetyl salicylic acid (ASA), IUPAC name: 2-Acetoxybenzoic acid, molecular formula: $C_9H_8O_4$) use is linked to a 53% reduction in all mortality among COVID-19 patients, according to data compiled from five trials. The usage of aspirin was shown to be related to a 49% reduction in in-hospital mortality among COVID-19 individuals who were hospitalized. Because of the wide use of this drug, we will review photocatalytic degradation solutions to its pollution problem as follows:

In one of the conducted research projects [66], the goal was to improve the UV/ZnO photocatalytic method for removing aspirin from aqueous solutions. To create the test procedure, the response surface methodology (RSM) program was used in this case. In this procedure, the effects of effective factors include the initial concentration of ASA (10–100 mg/L), contact duration (10–120 min), pH solution (3–11), and catalyst dosage of ZnO (100–600 mg/L) were studied. According to the findings, the greatest aspirin removal efficiency of 83.11% was achieved when the solution pH was 5.05, the contact duration was 90.50 min, the ZnO catalyst dosage was 375.16 mg/L, and the initial ASA concentration was 33.84 mg/L. Under ideal conditions, increasing the phosphate and chloride ion concentrations in a synthetic solution resulted in reduced and enhanced efficiency of the UV/ZnO process, respectively. The pseudo-first-order model exhibited the best association with ASA elimination utilizing the photocatalytic process of UV/ZnO (R^2 = 0.99), according to the kinetic studies. The UV-based ZnO photocatalytic method showed a great capability for removing ASA from aqueous solutions and may be utilized as an efficient, cheap, and easy-to-operate alternative on a large scale.

In another study, D. Mukherjee et al. [67] found out that under solar light irradiation, aspirin was degraded photocatalytically when TiO_2-filled polymeric film was present as a photocatalyst. The polymeric film contains TiO_2, which acts as a photocatalyst, degrading ASA into a range of organic compounds when exposed to sunlight before full demineralization (creation of water and carbon dioxide as end products). The presence of acetic acid was detected in greater quantities among the intermediates than other organic acids. The quantitative/qualitative studies of the intermediates led to the identification of the most likely degradation reaction mechanism. Using LC/MS, UV spectrophotometric investigation, and FTIR, the mechanism of acetylsalicylic acid degradation and its reaction route were discovered. In comparison to the electrons and holes created by TiO_2, hydroxyl

groups were shown to be more important in the degradation process. The amount of organic carbon in the intermediates produced throughout the breakdown process was also determined using a total organic carbon (TOC) assay.

Bianchi et al. [68] looked at the usage of a commercial micro-sized TiO_2 (anatase/rutile: 80/20) catalyst (K1077 by Kronos) in sewage treatment due to its non-toxic nature to both living things and the environment, as well as the powder's ease of handling, reuse, and recovery. The experimental circumstances highlight the complexities of heterogeneous photodegradation processes, including adsorption stages, competition among by-product nature, mixed pollutants, and medium influence. These impacts are confirmed and emphasized by our findings: 1-The drug-degrading ability of the micro-sized catalyst has been demonstrated. When compared to the nano-sized one, the photodegradation findings are virtually identical after 6 h and follow the same route. The presence of a micro-sized K1077 sample, on the other hand, causes the mineralization process to be significantly slowed down. 2-The paracetamol route is affected by the keto-enolic tautomeric equilibrium of benzoquinone/hydroquinone, and the mineralization trend follows the concentration of hydroquinone. 3-Because of their mutual rivalry on the catalytic surface, aspirin solvation influences the first adsorption phase, which is visible when combined with paracetamol. 4-In comparison to deionized water, the photodegradation, and mineralization processes are slowed by the tap water matrix. Both single and combined pollutants have the same photodegradation tendencies as the adsorption stages are even off. Mineralization degrees continue to fall, making it more difficult to remove contaminants such as CO_2 and H_2O.

The degradation of aspirin was used to examine the photocatalytic performance of P25-TiO_2, and the reaction system has been enhanced in a methodical manner using central composite design (CCD) and RSM in research by Li et al. [69]. In addition, three factors were chosen to examine the dependency of aspirin degradation efficiencies: the initial concentration of ASA, the initial value of pH, and the P25 concentration. Meanwhile, using analysis of variance (ANOVA), a projected model of breakdown efficiency was approximated and validated. The results showed that all of these factors, in decreasing order, had a substantial impact on the elimination of aspirin by P25: Initial concentration of ASA > P25 concentration > initial pH value. Furthermore, the CCD technique was used to improve the settings. By using P25-TiO_2 with a concentration of 50 mg L^{-1} and an initial pH value of 5, the breakdown efficiency of the ASA (with an initial concentration of ~10 mg/L) was found to be ~98.9% under 60 min irradiation of a Xenon lamp. Furthermore, two primary photocatalytic-based degradation routes of ASA by P25-TiO_2 were identified and a putative photo-degradation mechanism was postulated based on LC-MS data.

2.3. Ibuprofen

Ibuprofen ((IBP), IUPAC name: (RS)-2-(4-(2-methylpropyl)phenyl)propanoic acid, molecular formula: $C_{13}H_{18}O_2$) should not be used in patients with signs of COVID-19, according to French officials, which issued a warning in March 2020. This recommendation was based on unsubstantiated anecdotal accounts of severe COVID-19 patients being given ibuprofen [70]. There is currently no scientific evidence that ibuprofen increases the SARS-CoV-2 infection incidence or the COVID-19 severity. Like other NSAIDs, Ibuprofen has been widely used for controlling COVID-19. The photocatalytic degradation of Ibuprofen has been discussed in the following.

Bismuth oxychloride (BiOCl) has exhibited superior removal efficiencies, making it a viable alternative visible light photocatalyst as compared to conventional photocatalysts [71]. However, the mechanisms that cause BiOCl photodegradation are not well understood. In this regard, Arthur et al. [72] employed LC-MS/MS analysis to establish the routes through which IBP can be eliminated from water using the BiOCl photocatalyst. BiOCl changes IBP to two main photochemical compounds, 4-isobutylacetophenone (IBAP) and 1-(4-isobutylphenyl)ethanol (IBPE), according to LC-MS/MS and HPLC-DAD analysis. The IBP's carboxylic acid group interacts with holes (e^+) in the valence band, resulting in increased reactivity for BiOCl. In BiOCl photocatalytic degradation studies, no

hydroxylated-IBP was identified, which was easy to anticipate in a procedure prompted by the production and reactivity of reactive oxygen species (ROS). These findings were utilized to develop a photocatalytic breakdown path for ibuprofen, emphasizing the necessity of investigating both primary and secondary degrading processes while doing photocatalytic research.

Based on the results found by Liu et al. [73], an efficient method for enhancing the photocatalytic activity of BiOX is its doping by heterogeneous atoms. In this regard, S-doped BiOBr (S–BiOBr) was made in the absence of water using a solvothermal technique, which is expected to replace O in the lattice with S^{2-}. The photocatalytic breakdown of IBP, an example of an anti-inflammatory drug, is the first application for this material. S–BiOBr has a significantly greater degrading efficiency than pure BiOBr. The kinetic constant of S–BiOBr degradation (2.48×10^{-2} min^{-1}) is about three times bigger than pure BiOBr (0.83×10^{-2} min^{-1}). The band structure of BiOBr is tuned by S-doping, resulting in a smaller bandgap and therefore a greater visible light usage efficiency. The production of H_2O_2 and OH radicals is thought to be responsible for ibuprofen breakdown on S–BiOBr. The OH radical, in conjunction with holes, plays a synergistic function in the process of photocatalytic degradation, which is said to be superior to the previously described superoxide- or single hole-dominant reaction. The results of this study provide a previously unknown and much more effective technique for organic pollutant breakdown on BiOBr.

Besides Ibuprofen, waste used tires are also a major environmental concern owing to hazardous chemicals seeping into soils and water. Furthermore, exposure to environmental circumstances might render them carriers for vectors such as mosquitoes. The sol–gel technique was used to manufacture three activated carbon (AC) catalysts generated from titanium dioxide (in both anatase and rutile phases), silver, and waste tire rubber in [74]. The aggregation of silver crystals and titanium particles on the surface of the AC was visible in morphological characterizations such as TEM and SEM. The existence of elemental silver nanoparticles was discovered via XRD analysis. A reduction in the titanium band gap was observed, in addition to visible spectrum activities using diffuse reflectance spectroscopy. The photocatalytic experiments were conducted in the presence of UV/Vis light at pH 3 and 7. In both the UV and visible areas, these tests reveal variations in the catalyst. Ibuprofen is removed primarily by adsorption, followed by photolytic degradation. The catalysts have excellent performance for removing ibuprofen in the visible spectra.

In another research, Romeiro et al. [75] made a comparison between the naproxen (NPX) and IBP photocatalytic degradation by TiO_2 nanoparticles in water. Photocatalysts made by various techniques were compared and tested to commercially accessible Evonik-P25 TiO_2 as well as direct photodegradation. The produced nanoparticles had strong photocatalytic activity against NPX (>90% degradation) and IBP (>97% degradation), with NPX mineralization reaching up to 79% and IBP mineralization reaching about 50%. IBP photoproducts included 1-(4-ethylphenyl)-2-methylpropan-1-ol, 1-(4-isobutylphenyl)ethanol, and 1-(4-isobutylphenyl)ethanone, whereas NPX photocatalysis produced 1-(6-methoxynaphthalen-2-yl)ethanone and 1-(6-methoxynaphthalen-2-yl)ethanol. The findings were explained by examining one important principal route, which includes decarboxylation of a chemisorbed molecule first, then breaking down of the radical intermediate generated. These results clearly imply that the degradation mechanism for these carboxylic acid-containing compounds involves a challenge between chemisorbed substances' oxidative decarboxylation by hydroxyl radical attack on physisorbed substrates when these substances have carboxylic acid groups and semiconductor holes.

In another investigation [76], the photocatalytic degradation of IBP was studied using Cu-doped $LaFeO_3$ and $LaFeO_3$ nanopowders. In the presence of the catalyst and H_2O_2, IBP aqueous solutions were exposed to visible light. The tests were done with aqueous solutions containing 5.0×10^{-5} M IBP, 0.130 g L^{-1} (5.0×10^{-4} M) catalyst, and 0.003 M H_2O_2. The composition of the reaction fluid was examined using UV-Vis spectroscopy and HPLC. Cu-doped $LaFeO_3$ (5 and 10 mol%) had greater photocatalytic activity than pure $LaFeO_3$, according to the findings. When employing a 5 mol% Cu-doped $LaFeO_3$

catalyst, the 4-isobutylacetophenone (4-IBAP) concentration, which is a hazardous IBP breakdown by-product, was the lowest, that is, ~2% and much less than 1% of the IBP original concentration after 5 and 24 h of irradiation, respectively. The proportion of IBP and 4-IBAP degradation was reduced by using a chloride water matrix.

The breakdown and mineralization of ibuprofen by using TiO_2 (80% anatase and 20% rutile) photocatalysts exposed to UV LEDs were studied by Jallouli et al. [77]. The TiO_2/UV-LED system was utilized to analyze ultra-pure water samples (UP), a retreated sewage from a municipal wastewater treatment plant (WWTP), and an extremely concentrated IBP water (230 mg L^{-1}) a pharmaceutical industrial wastewater (PIWW). The number of LEDs, catalyst load, and pH of the solution were all adjusted as operational parameters. HPLC and ultra-high-performance LC linked to tandem MS (UHPLCMS/ MS) were used to obtain the effectiveness of the procedure in terms of IBP elimination. The amount of dissolved organic carbon (DOC) was also measured to further explore the mineralization. Based on data acquired utilizing LC having a high-resolution mass spectrometer ion trap/time-of-flight (LC-MS-IT-TOF), the chemical structures of transformation products were postulated. As a result, a potential mechanism for IBP degradation was proposed. To assess the acute toxicity of both treated and untreated effluent, conducting bioassays by marine bacteria Vibrio fischeri is a way. TiO_2 heterogeneous photocatalysis was effective in removing IBP from PIWW and UP but less so in treating municipal WWTP effluent. Regardless of the investigated matrix, acute toxicity decreased by around 40% following therapy.

Tanveer et al. [78] used photocatalytic-based oxidation processes to explain the breakdown of IBP to intermediates and then carbon dioxide and water. The irradiation-activated catalysts were TiO_2 (anatase phase) and ZnO exposed to UV or sunlight simulator irradiation. Borosilicate tubes and quartz were employed in the solar reactor to absorb the needed ultraviolet radiation, while reflection and focusing of the light on the feed mixture tubes were conducted using curved chrome plates. To assess the rates of deterioration and demineralization of solution samples, liquid chromatography, TOC, and COD tests were used. TiO_2-based studies demonstrated a significant rate of deterioration under acidic environments at catalyst dosing of 1 mg/L to 1.5 mg/L. Under neutral circumstances (pH = 7.0), a 1 mg/L dozing rate for ZnO catalyst was shown to be effective. When compared to a solar reactor, UV lamp-based photocatalysis exhibited a greater degradation rate. Furthermore, because quartz tubes absorb more solar radiation, they degrade more quickly than borosilicate tubes. The TOC and COD reductions were greater with UV light photocatalysis. Solar-based degradation of IBP might be more efficient than UV-based catalysis with better solar reactor design and catalyst doping.

One of the most effective techniques for degrading new contaminants such as Ibuprofen is to use an advanced oxidation process. To treat synthetic wastewater containing IBP, Shafeei et al. [79] built a batch reactor using LED lamps, TiO_2, and modified TiO_2. They used 0.5, 2, and 5 mg of the IBP, 0.05, 0.1, 0.15 of the TiO_2, 0.2, 0.3, 0.4 g of the modified TiO_2, pH values of 5, 7, and 9, and exposure times of 0.5, 1, 2, 3, 4, 5, and 6 h. For removing IBP from synthetic wastewater, they used the optimal amounts of FeFNCS-TiO_2 and TiO_2 of 0.2 and 0.3 g, respectively. In FeFNS-TiO_2/LED and TiO_2/LED processes, respectively, they achieved 91.4% and 52.4% IBP breakdown efficacy in synthetic sewage, at pH 7, 3 h radiation duration, and IBP concentration of 0.5 mg/L. The research on synergistic effects also revealed that the photocatalyst and LED had a beneficial impact on each other. When tert-butyl was added to the solution of IBP as a radical scavenger, the removal capability in the TiO_2/LED and FeFNS-TiO_2/LED processes decreased by 23.8% and 37.3%, respectively. This work might point to the hydroxyl radical-mediated photocatalytic breakdown of IBP. The first-order model of Lagergren was fitted in a condition with pH values of 7 and 5, exposure times of 1, 2, 3, 4, 5, and 6 h and 0.5 mg L^{-1} concentration of the IBP, 0.2 g of the modified TiO_2, 0.3 g of TiO_2. TiO_2/LED and modified TiO_2/LED have kinetic rate constants of 0.0591 and 0.123, respectively.

Due to the importance of low-concentrated contamination of water resources, the photocatalytic breakdown of IBP at low ppm levels was also investigated using a zinc

oxide-based catalyst. The goal of the investigation [80] was to see how well IBP was degraded by a heterogeneous ZnO photocatalyst when exposed to UV-C. Field emission SEM (FE-SEM) and XRD were used to examine the photocatalyst. Under VU-C irradiation light, in a cylindrical glass reactor, ZnO nanoparticles' photocatalytic activity was studied. Modeling and optimization of IBP breakdown under various factors such as starting pH, initial concentration of IBP, ZnO loading, the concentration of humic acid, and reaction time were done using CCD and RSM. The reaction time had the most favorable influence on IBP degradation, according to the findings of our studies. The correlation coefficient, R^2 = 0.856, suggested that the experimental data and model predictions were in excellent accordance. The highest IBP degradation was achieved at pH 6.7, initial concentration of IBP 1.5 mg/L, catalyst concentration of 583 mg/L, humic acid (54 mg/L), and reaction duration of 95 min, according to optimization findings. They found an IBP removal effectiveness of 82.97% under these conditions. Finally, ZnO was discovered to be an excellent photocatalyst and a viable option for generating $^{\bullet}$OH for the breakdown of IBP, which is an increasing contaminant in water resources.

In another investigation [81], the PAN/MWCNT composite nanofibers were effectively crosslinked with TiO_2–NH_2 NPs. The manufactured PAN-MWCNT/TiO_2–NH_2 nanocomposites were shown to be an efficient photocatalyst for IBP, CIZ, and NPX breakdown in aqueous-based solutions under UV irradiation in this study. The initial concentration of the drug, quantity of catalyst, irradiation period, and pH of solution were all studied as operational factors. Complete degradation was demonstrated using a modest concentration of drug (5 mg/L), a low UV light power intensity (40 Watt), and an acidic pH of 2. IBP, NPX, and CIZ were photodegraded completely in 120, 25, and 40 min, respectively. The photodegradation efficiency of the PAN-MWCNT/TiO_2–NH2 nanofibers remained constant in the case that the experiment was done, according to the stability studies.

The efficiency of TiO_2 photocatalyst (anatase phase) for the elimination of ibuprofen from the aquatic environment was examined by Khalaf et al. [82]. Two investigations were carried out with TiO_2 in heterogeneous photocatalysis: (1) dispersed powder, and (2) coating on a glass surface. The photoreaction kinetics were calculated, and the photoproducts were identified using LC combined with Fourier-transform ion cyclotron resonance mass spectrometry (LC-FTICR MS). The findings indicated that recovery difficulties can be avoided by immobilizing the TiO_2 active powder as a thin layer on a glass substrate. They supposed that this process can be considered a useful technique for environmental protection from emerging pollutants like ibuprofen and its derivatives.

In another investigation regarding the IBP removal from water resources by applying the oxidation treatments, IBP's photocatalytic degradation with TiO_2 nanoparticles and UV light, as well as g-C_3N_4 nanosheets and visible light, are suggested and analyzed [83]. The by-products of both photocatalytic systems were detected by UHPLC and high-resolution MS techniques, using a quadrupole-time of flight mass spectrometer in both modes of ionization (positive and negative), which enabled the basic composition of their fragment ions and precursors to be determined. At three pH levels, the elimination of ibuprofen and the production of by-products were investigated. Depletion of IBP followed pseudo-first-order kinetics, which has rate constants of 0.04, 1.0, and 0.0006 min^{-1} for TiO_2/UV at pH values of 2.50, 5.05, and 12.04, and for the g-C_3N_4/vis 0.03, 0.007, and 0.0005 min^{-1} at pH values of 2.51, 5.05, and 11.33, respectively. A total of 18 by-products were discovered, with minor variations from one photocatalytic system to another. The development of the most prevalent by-products (tentatively designated as 1-(4-isobutylphenyl)ethan-1-ol, 1-(4-ethylphenyl)-2-methylpropan-1-one, 1-(4-acetylphenyl)-2-methylpropan-1-one), and 1-(4-ethylphenyl)-2-methylpropan-1-ol was studied and the findings backed up chemical pathways that involved OH radical attacks accompanied by decarboxylation. Furthermore, several by-products of the photocatalytic oxidation of ibuprofen have been described for the first time.

2.4. Naproxen

Naproxen ((NPX), IUPAC name: (+)-(S)-2-(6-Methoxynaphthalen-2-yl)propanoic acid, molecular formula: $C_{14}H_{14}O_3$) is an NSAID that is used to treat pain, menstrual cramps, and inflammatory illnesses including fever, gout, and rheumatoid arthritis, among other things [84,85]. Naproxen has been found in all forms of water, such as groundwater and drinking water, at this time. The concentrations found varied from ng/L to µg/L. Even while these quantities are modest, long exposure to nontarget species may be harmful, particularly when naproxen is combined with other medicines so proper degradation of this drug is important [86].

The most useful substances for UV-mediated photodegradation of stubborn contaminants in sewage are oxide semiconductors. Even though lots of research have been published to date on the PC activity of TiO_2 (anatase phase) and ZnO, the capability of mixed oxides in breaking down a great variety of organic contaminants has yet to be thoroughly investigated. In [87], researchers evaluated the decomposition efficiency of a dye (methylene blue) and a pharmaceutical (NPX) using ZnO, TiO_2, and the ZnO–TiO_2 mixed production obtained by the mechano-chemical solid-state method. The nanopowders' composition, phase morphology, crystalline structure, and specific surface area were all studied in depth. Under the irradiation of UV light, ZnO's photocatalytic activity was consistently greater than that of the other substances. The mixture activity was shown to be influenced by the kind of analyte molecule used, although it was found to be greater than that of clean TiO_2 nanoparticles.

Nanoscale γ-FeOOH was produced and applied for photodegradation of NPX [88]. THe γ-FeOOH nanostructures have the ability to photodegrade NPX quickly under UV irradiation. The rate of photodegradation of NPX was affected by γ-FeOOH concentration in the solution, the initial concentration of the NPX, and the pH of the solution. The photodegradation rate of NPX was raised and then stabilized as the concentration of γ-FeOOH was increased. In addition, in acidic conditions, the NPX photodegradation was observed at its fastest rate. It was discovered that the photocatalytic mechanism of NPX breakdown on γ-FeOOH is a semiconductor-based photocatalysis, according to electron spin resonance properties of active chemicals (such as OH, h^+, e^-, $^1O_2$, and ($^{\bullet}O_2^-$).

In a recent study, Fan et al. [89] presented a high performance TN photocatalyst that was modified with H_2O_2 (HTNM) with a high photo-response to photocatalytic activity and visible light irradiation. The findings demonstrate that H_2O_2-modified TNs may significantly increase photocatalytic activity and visible light absorption. The HTNM can remove 99.9% of NPX in 180 min when exposed to visible light. The rate of degradation was evaluated by using a pseudo-first-order kinetics model, and the catalytic activity was found to be constant. Cl, CO_3^{2-}, SO_4^{2-}, and NO_3^- hindered the photodegradation of NPX in an aqueous solution. NO_3^- had the largest influence on NPX degradation, and others were CO_3^{2-}, SO_4^{2-}, and Cl. Fulvic acid (FA). A prevalent humus in water would slow down the breakdown of NPX, but humic acid (HA) may speed up the NPX photocatalytic breakdown. The mechanism analysis revealed that the photodegradation of NPX by the HTNM was mostly mediated by $^{\bullet}OH$ and O^{2-}, with hydroxylation and decarboxylation being the NPX degradation primary routes, take a look at Figure 3. In conclusion, the HTNM provides a superior method of photocatalytic degradation for eliminating NPX in aquatic settings than pure titanate, gives a new approach for treating NPX-contaminated sewage, and can present widespread applications in aquatic-based environments.

Kanakaraju et al. [90] proposed a mixture of two NSAIDs, NPX, and diclofenac (DCF) degradation by using an immersion-well photoreactor, TiO_2-mediated solar photocatalysis (80% anatase and 20% rutile), and solar photolysis. Solar degradation was used to test both NSAIDs at an equimolar ratio (1:1) in river water, drinking water, and distilled water. Because both medicines may experience photolysis, the mixture of NPX and DCF solar photolysis was competitive, especially in rivers and drinking water. In comparison to solar photolysis alone, adding TiO_2 to the mixture dramatically increased the rate of degradation of both APIs. Under all circumstances studied, mineralization was incomplete as assessed

by chemical oxygen demand (COD). LC-MS and LC-FTICR MS were used to identify two products of degradation with greater molecular mass than the initial NSAIDs. Degrading the mixture of NPX and DCF using TiO_2-mediated solar photocatalytic breakdown has generated 15 recognizable degradants relating to the breakdown of each of the NSAIDs. The total effectiveness of TiO_2-mediated solar photocatalysis and solar photolysis for breaking down the mixtures of NPX and DCF appears to be influenced by the intensity of the water matrix and solar light, according to this study.

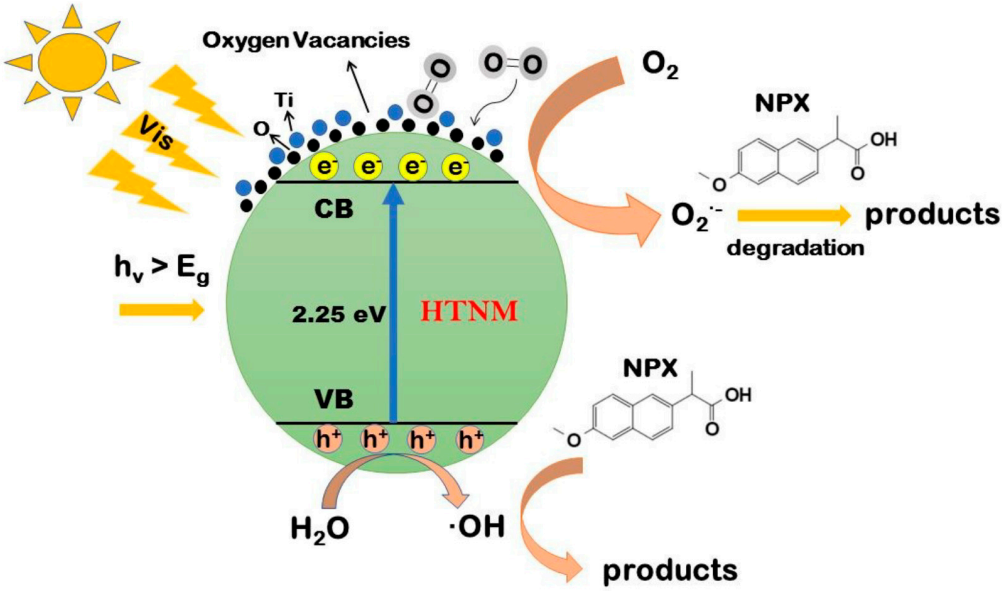

Figure 3. The possible mechanism describing the photocatalytic degradation of NPX by HTNM in the presence of visible light irradiation. Reprinted/adapted with permission from Ref. [89]. Copyright 2019 Royal Society of Chemistry.

Jallouli et al. [91] investigated TiO_2-photocatalytic breakdown and direct photolysis of naproxen in an aqueous solution under solar and UV light irradiation. The photocatalytic procedure was shown to be more effective than photolysis in the degradation of the NPX, which followed pseudo-first-order kinetics. After 3 h, photolysis (initial pH of 6.5) removed 83% of NPX and reduced 11% of COD, while the TiO_2-UV process removed both COD (25%) and NPX (98%). For photolysis of NPX, the measured first-order rate constant ranged from 0.0050 min^{-1} to 0.0095 min^{-1} at pH 3.5 and 6.5, respectively, but it was calculated to be 0.0063 min^{-1} in photocatalysis under acidic circumstances, rising by four-fold at pH 6.5. To identify NPX degradation products, researchers utilized UHPLC with a triple quadrupole detector, as well as a hybrid mass spectrometer that integrates the OrbiTrap mass analyzer and linear ion trap triple quadrupole (LTQ). 2-ethyl-6-methoxynaphthalene, 1-(6-methoxynaphtalen-2-yl) ethylhydroperoxide, 1-(6-methoxynaphtalen-2-yl) ethanone, 1-(6-methoxynaphtalen-2-yl) ethanol, and malic acid were the major intermediates found. After 3 and 4 h of treatment, NPX solar photocatalysis revealed COD reductions of 33 and 65%, respectively, as well as some decrease in acute toxicity, as measured when *Eisenia andrei* was exposed to OECD soils that had been spiked with NPX-treated solutions.

In another work [92], the elimination of NPX by using a UV-based ZnO photocatalytic system was investigated. The influence of some variables, including ZnO content, contact duration, pH, temperature, and initial concentration of NPX, was investigated. The adjusted R^2 = 0.9843 and projected R^2 = 0.9695 coefficient values were also high in the ANOVA findings. To forecast the NPX elimination effectiveness of the UV/ZnO processes, the quadratic model that has the greatest R^2 designation was used. The NPX removal efficiency of 71.19% was found under ideal circumstances, which included an optimum initial concentration of NPX that is 21.59 mg/L; a concentration of ZnO, which is 371.15 mg/L; pH of 6.87; contact duration of 73.92 min; and temperature of 24.35 °C. The results reveal

that the factors starting NPX content, time, pH, and ZnO concentration have the greatest influence on the removal of NPX, whereas temperature has little impact on the effectiveness of the process. Furthermore, the pseudo-first-order model may be used to explain the NPX photodegradation kinetics. The UV/ZnO photocatalytic technique has a great capability for removing NPX, and CCD is an excellent method for optimizing NPX photodegradation operating conditions.

The practical application of photocatalysts in the breakdown of NPX is still limited due to difficulties such as the necessity for UV light to activate most nanomaterials and their low visible light photocatalytic activity. As a result, G. Fan et al. [93] used a two-step hydrothermal-calcining technique to create bismuth titanate nanobulks (Bi-TNB). The initial concentration of NPX, dosage of catalyst, pH of the solution, and concentrations of cations, anions, and humus were all investigated as potential influences on degradation efficiency. Bi-TNB (0.5 g L^{-1}) eliminated more than 99.9% of NPX (0.25 mg L^{-1}) at pH = 7, according to the results. $^{\bullet}O_2^-$ and h^+ were the major active species that took part in the breakdown of NPX, according to reactive species scavenging studies. NPX was initially decarboxylated during the photodegradation process, then photocatalytically oxidized to generate lower molecular weight carboxylic acids, which were subsequently converted to CO_2 and H_2O. Acetaminophen inhibited the elimination of NPX by Bi-TNB in the PPCPs coexistence experiment. Bi-TNB might be used to degrade NPX in environmental water systems, according to both the response in various water matrices and the breakdown under sunshine conditions. This research proposes a novel method for improving material photocatalytic performance that may be applied in real-world situations.

The advancement of photocatalysts that respond to visible light is critical for dealing with the energy problem and environmental cleanup. In this regard, a one-pot hydrothermal technique was used to make reduced graphene oxide/$ZnIn_2S_4$ (rGO/ZIS) as a visible light-driven photocatalyst for the degradation of naproxen [94]. The rGO/ZIS nanocomposite showed a remarkable degradation efficiency (~99% within 60 min visible light irradiation). The high light absorption capacity and efficient photoinduced e-h pair separation of the samples were proposed as the main agents contributing to the improvement of the photocatalytic degradation performance. The photocatalytic degradation processes are dominated by hole (h^+) and superoxide radical ($^{\bullet}O_2^-$), according to the reactive species quenching studies and EPR measurements. Degradation intermediates were also discovered, and a degradation route was proposed.

3. Mucolytics

Mucolytics are medications that make mucus thin and less sticky, making coughing easier. They can assist in coughing out mucus from the lungs in a situation of chronic (long-term) cough [95,96].

Ambroxol

Ambroxol ((AMB), IUPAC name: trans-4-[(2-Amino-3,5-dibromobenzyl)amino] cyclohexanol, molecular formula: $C_{13}H_{18}Br_2N_2O$) is a medication that is widely used to prevent chronic bronchitis. The interaction between the Receptor Binding Domain of the Coronavirus 2 Spike Protein and Recombinant Human ACE2 is inhibited by ambroxol hydrochloride [97]. This stubborn chemical becomes a dangerous contaminant if it is discharged into surface water. Tab et al. [98] examined the capacity of 1% Mn-doped TiO_2 (Mn-TiO_2 (in both anatase and rutile phases)) to photocatalyze the mineralization of AMB. In the presence of UVA light, for 30 min, complete degradation of the AMB (30 ppm) was achieved using Mn-TiO_2 at a dosage of 0.625 g L^{-1} at pH 7, whereas complete mineralization in CO_2 (more than 96%) was obtained after 24 h. Mn-TiO_2 outperformed TiO_2 Degussa P25 by 1.6 times. LC with electrospray high-resolution MS was also used to investigate the products. The researchers found 21 photodegradation products and characterized them. Additionally, ionic chromatography studies indicated that 97, 35, and 63% of the Br and N originally contained in the AMB were released as Br^-, NO_3^-, and NH_4^+, respectively.

Finally, the photocatalyst's reusability was investigated. The virtually total photodegradation of AMB was accomplished after four cycles, demonstrating that the Mn-TiO_2 was significantly stable. This research adds new physicochemical properties to the Mn-TiO_2 photocatalyst. It is also the first research to look at the photocatalytic breakdown of the resistant AMB medicine.

4. Antibiotics

Antibiotics are ineffective in treating COVID-19, which is caused by the novel coronavirus, according to WHO. Antibiotics are only effective against bacteria, not viruses. Doctors may give antibiotics for subsequent bacterial infections if individuals are undergoing COVID-19 therapy in the hospital. This wide usage of antibiotics has caused environmental contamination. Pharmaceutical industry effluents have been identified as important contributors to antibiotic-related aquatic contamination. Although such contamination has mostly been documented in Asia, information about industrial discharges in other parts of the world, including Europe, as well as the consequences of such exposures, is still restricted [99]. Antibiotic residues in the environment can have damaging consequences on biota at various trophic levels, as well as human health, by contaminating food and water, contributing to the growth of resistant bacteria, and retaining selective pressure that leads to dissemination and/or development of resistance in various compartments of the environment [100]. Antibiotics show some side effects on the human body, such as diarrhea, nausea, and stomach pain. In some cases, they also cause kidney stones, abnormal blood pressure resulting in clotting, sensitivity to sunlight, and allergies.

4.1. Azithromycin

Azithromycin ((AZY), IUPAC name: (2R,3S,4R,5R,8R,10R,11R,12S,13S,14R)-2-ethyl-3,4,10-trihydroxy-3,5,6,8,10,12,14-heptamethyl-15-oxo- 11-{[3,4,6-trideoxy-3-(dimethylamino)-β-D-xylo-hexopyranosyl]oxy}-1-oxa-6-azacyclopentadec-13-yl 2,6-dideoxy-3C-methyl-3-O-methyl-α-L-ribo-hexopyranoside, molecular formula: $C_{38}H_{72}N_2O_{12}$), a licensed, widely accessible, inexpensive, and generally safe antibiotic, has been suggested as a therapy for COVID-19, with in-vitro studies indicating efficacy against several viruses, including SARS-CoV-2. Azithromycin may raise the pH of the Golgi network and recycle endosomes, causing SARS-CoV-2 activity and replication to be disrupted. The medication may also lower levels of the enzyme furin, which might make it harder for SARS-CoV-2 to enter cells because the virus's spike protein is thought to have a furin-like cleavage site. The capacity of azithromycin to lower the levels of proinflammatory cytokines like IL-6 may limit the potential of SARS-CoV-2 infection to cause a cytokine storm and tissue damage. Because of the wide use of azithromycin against coronavirus, one way of cleaning the environment from this drug is its photocatalytic degradation.

In research [101], nanostructured TiO_2 film was produced by using titanium tetraisopropoxide in a dip-coating sol-gel approach followed by a heat treatment at 550 °C. The TiO_2 thin film was discovered to be made entirely of the anatase phase and to have a microscale granular morphology. The most efficient degradation technique for possible application in wastewater treatment was determined by studying the photocatalytic breakdown of azithromycin using the TiO_2 nanostructures. During photocatalysis, several variables including water matrix and pH (3, 7, and 10) were assessed (synthetic municipal sewage and ultrapure water), along with the effect of another active medicinal ingredient (sulfamethoxazole, one of the most common pharmaceutical chemicals found in waste waterways), and radiation sources (ultraviolet (UV) mercury lamps with UV-A and UV-C ranges; an LED lamp whose radiation peak is 365 nm). In matrices with a pH of 10, the most successful breakdown process was obtained using the UV-C irradiation source. Azithromycin photocatalytic breakdown rates were unaffected by the water matrix. The sulfamethoxazole inclusion in the water matrices having pH~10 reduced the degradation rate of azithromycin. Azithromycin breakdown products were discovered to be five throughout the tests, and none of them were hazardous, indicating that azithromycin was effectively

removed. The UV-C lamp was more effective than the LED 365 nm irradiation source. However, given the energy efficiency, cost, and environmental features of the radiation sources, the LED light would be a practical "real-world" solution.

In another work [102], La-doped titania/active carbon nanocomposites (La-TiO_2/AC) were produced through a sol-gel technique for photocatalytic degradation of azithromycin and studied using BET and SEM. A UV lamp serves as the light source for a photocatalytic reactor and La-TiO_2/AC as the photocatalyst was used to clean azithromycin wastewater. The results reveal that at pH = 4, 10 mg L^{-1}, and a reaction period of 90 min, the azithromycin's rate of degradation reached 95.6%. The La-TiO_2/AC photocatalyst rate of deterioration, which was reused 15 times, remained over 95%. More research was done to investigate the procedure of azithromycin photocatalytic degradation mediated by La-TiO_2/AC. The outcomes reveal that the major intermediates in the observed photocatalytic process are desosaming lazithrocmycin. As an advantage, the carbon- or silver-containing TiO_2-based photocatalysts are able to completely degrade and inactivate the residual bacteria that remained in the hospital wastes and drugs under solar light irradiation [45,103].

Naraginti et al. [104] used a simple hydrothermal and photodeposition technique to create a new ZrO_2/Ag@TiO_2 (anatase phase) nanorod ternary nanocomposite for effective AZY degradation under visible light, degradation mechanism is shown in Figure 4. XRD, XPS, and TEM studies were used to describe the composite, which indicated the production of cubic ZrO_2 and Ag NPs on TiO_2 nanorods (TNR). After an 8-h exposure to visible light, more than 90% of AZY (20 mg L^{-1}) was broken down. According to the LC/MS-IT-TOF study, a feasible transformation route for azithromycin was presented. On Vigna radiata, the phytotoxicity of AZY and its degradation metabolites was evaluated. The AZY germination index (GI) before breakdown was discovered to be 12.3% and after 8 h, it increased to ~81%, showing that the photodegradation process was virtually complete. The toxicity of the breakdown products was also evaluated using an Escherichia coli colony-forming unit test, which revealed high detoxifying effectiveness.

The major findings on the possible use of simulated sunshine and persulfate (PS) to remove AZY were presented in [105]. A face-centered, central composite experimental design was used to obtain the effects of solution pH and PS concentration. After 120 min of reaction, it was feasible to achieve an AZY removal of about 70% and a 30% reduction in total organic matter under optimal experimental circumstances. Furthermore, it was shown that AZY removal is favored by basic pH conditions and that large concentrations of PS may hinder the process owing to radical scavenging phenomena. The effects of the $^{\bullet}SO4^{-}$ and $^{\bullet}OH$ radicals on the reaction were studied in the presence of ethanol and tetra-Butyl alcohol in experiments. $^{\bullet}OH$ radicals appear to be the primary oxidizing species of AZY in this way. Finally, the influence of the starting pollutant concentration was investigated, allowing it to be determined that a pseudo-first-order kinetics model may be utilized to explain the removal of AZY under the tested experimental circumstances.

In another work [106], the hydrothermal technique was used to make molybdenum sulfide GO composites. The photocatalytic efficacy of molybdenum sulfide graphene oxide composites was tested for AZY in the visible light region due to their higher conductivity. After irradiation with visible light for three hours, the rates of degradation for molybdenum sulfide graphene oxide composites and molybdenum sulfide to 100 mg L^{-1} AZY were 75% and 87%, respectively. The ability of molybdenum sulfide graphene oxide composites to degrade AZY is better.

The goal of the study by Sayadi et al. [107] was to make graphene reinforced with nanocomposites of zinc oxide, iron oxide, and tin oxide and test its capability to degrade AZY photocatalytically in an aqueous solution. The XRD, TEM, FT-IR, and VSM methods were used to characterize the GO@Fe_3O_4/ZnO/SnO_2 nanocomposite. The impact of pH, contact duration, catalyst properties, and the initial concentration of AZY were examined in the batch system; in this system, 90.06% of 30 mg L^{-1} AZY were destroyed under UV-C exposure under optimum circumstances of pH = 3, 120 min, with 1 g L^{-1} of GO@Fe_3O_4/ZnO/SnO_2. The factors of flow rate, bed height, and AZY initial concentration

were studied in the continuous system. At heights of 6, 8, and 10 cm, the times to achieve the column breakthrough point (C_b = 0.02 C_0) were 5, 8, and 14 min, respectively. The AZY degradation rate increases when the bed height is increased from 6 to 10 cm; this increase might be attributed to a contact time increase. The outcomes show that AZY degradation in a constant bed column is highly influenced by these variables; in fact, As the flow velocity and initial AZY concentration grew, the time it needs to reach the breaking point dropped, while the time it took to reach the breaking point increased as the bed height increased. The model's prediction of vacant bed residence time was shown to be in excellent accord with laboratory findings. As a result of GO@Fe_3O_4/ZnO/strong SnO_2's capacity to remove azithromycin, this molecule can be employed as an efficient photocatalyst for the degradation of antibiotics in aqueous solutions.

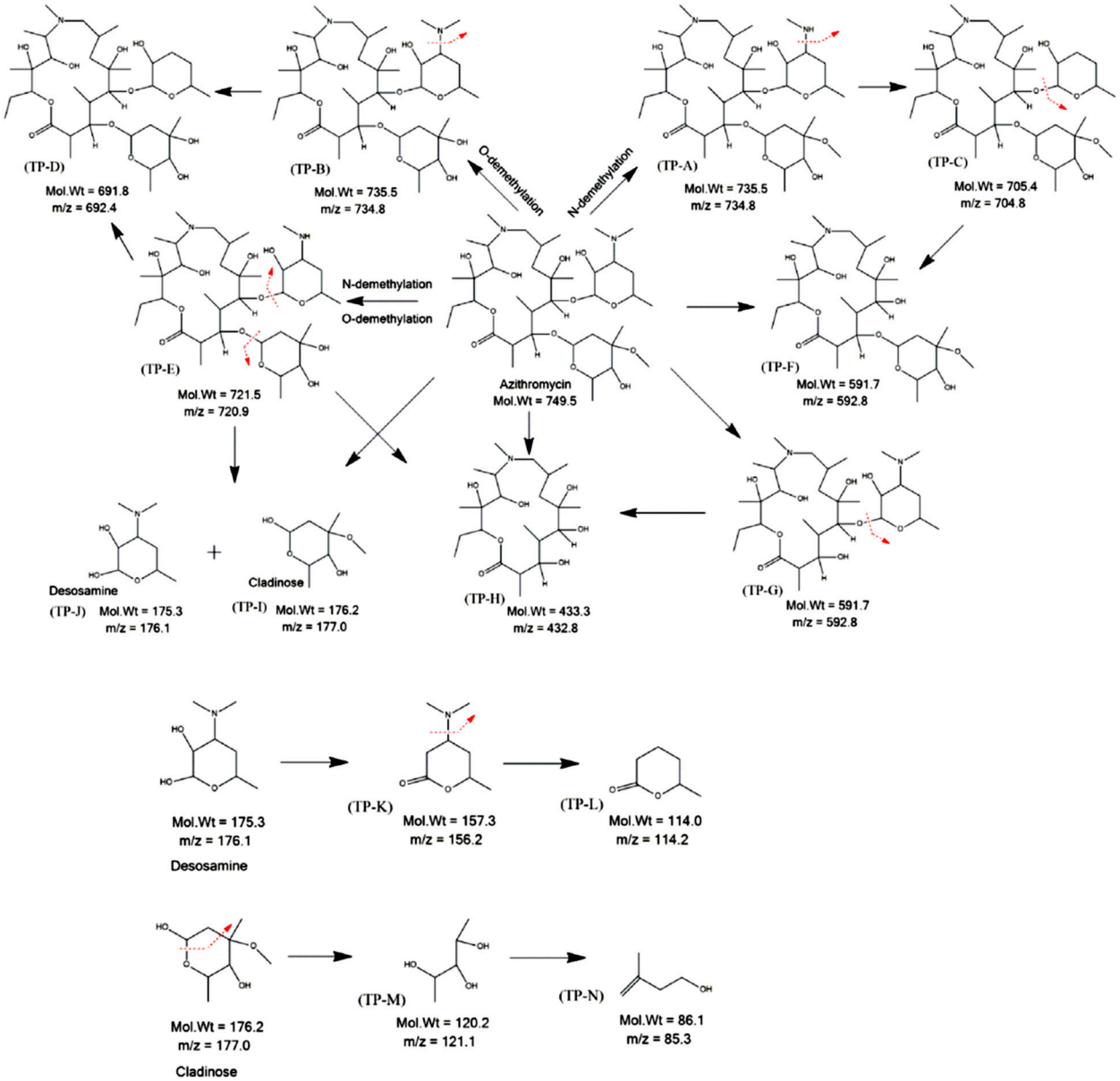

Figure 4. Possible degradation mechanism of azithromycin by ZrO2/Ag@TNR composite in the presence of visible light. Reprinted/adapted with permission from Ref. [104]. Copyright 2019 Elsevier.

4.2. Quinolones

Quinolones are antibiotics that can be used to treat a variety of microorganisms. They are known as broad-spectrum antibiotics because they block numerous distinct types of bacteria. They are also a great option if one is allergic to conventional antimicrobials like penicillin or macrolide antibiotics, which can be a problem in pneumonia instances [108] so proper degradation of this drug is crucial.

In work by Sirtori et al. [109], two solar photocatalytic procedures, photo-Fenton and TiO_2, were used to assess the breakdown of nalidixic acid (NXA) and Flumequine (FLU) in filtered and pure water. The photoproducts' intermediates and acute toxicity were also investigated. The degradation efficiency of NXA and FLU by heterogeneous photocatalysis with TiO_2 was identical, with both being fully destroyed after 25 min of irradiation. After 80 min of illumination, there was less NXA mineralization. Both compounds were photo-Fenton degraded quickly (<25 min), and the same mineralization was achieved in both situations. To compare their photocatalytic degradation, the kinetic characteristics of the two compounds were computed. As determined by a Vibrio fischeri bioassay, photocatalytic procedures were linked to lower toxicity in all situations. In addition, even though in the reaction solution, FLU, and NXA were still present (first samples), a significant reduction in inhibition was seen from the start of the therapy. These findings show that toxicity lowers considerably in both photocatalytic processes examined, resulting in a phototreated sample that is below acceptable toxicity limitations. LC-time of flight-MS (LC-TOF-MS) was utilized to study the intermediates generated through photocatalytic degradation.

Quinolones include chloroquine and hydroxychloroquine. Despite the fact that their medicinal and toxic doses differ, they are similar medicines with comparable clinical indications for usage and retinal toxicity symptoms [110]. The antimalarial medication chloroquine was first introduced in 1934. In 1946, an analog of chloroquine called hydroxychloroquine was created. In addition to treating malaria, hydroxychloroquine is also utilized to cure autoimmune diseases, including rheumatoid arthritis and systemic lupus erythematosus. Both chloroquine and hydroxychloroquine can raise endosomal pH, preventing SARS-CoV-2 from fusing with the host cell membrane. Chloroquine prevents the cellular angiotensin-converting enzyme 2 (ACE2) receptor from becoming glycosylated, which may prevent SARS-CoV from attaching to the receptor. Both chloroquine and hydroxychloroquine have been shown in vitro to inhibit the transfer of SARS-CoV-2 from early endosomes to endolysosomes, perhaps inhibiting the viral DNA from being released. Immunomodulatory actions of chloroquine and hydroxychloroquine have been proposed as another possible mechanism of action for the treatment of COVID-19 [111]. Therefore, we will discuss their degradation.

4.2.1. Hydroxychloroquine

In an interesting work, the goal of da Silva et al. [112] was to assess the ZnO catalysts' photocatalytic activity based on clinoptilolite, which is a natural zeolite, for hydroxychloroquine's ((HCQ), IUPAC name: 2-[4-[(7-chloroquinolin-4-yl)amino]pentyl-ethylamino]ethanol, molecular formula: $C_{18}H_{26}ClN_3O$) photocatalytic breakdown. The wet impregnation technique was utilized to make 15% ZnOCP and 10% ZnOCP catalysts. XRD, SEM, DRS, BET, XRF, FT-IR, PCZ, and PL were used to categorize the raw and manufactured catalysts. Before and after the photocatalytic procedure, the absorption of UV-vis from the samples was used to measure the degradation of hydroxychloroquine. With operating conditions of C_0 = 10 mg L^{-1}; C_{cat} = 2 g L^{-1} of 15% ZnOCP; pH = 7.5; UV-A light, the highest percentage of degradation (96%) was achieved. Ecotoxicological studies on the Artemia salina and bioindicators Lactuca sativa verified that effluent toxicity has decreased following treatment.

In another study [113], the breakdown of the HCQ drug in aqueous-based solutions was studied using electrochemical oxidation methods such as sonication (sono-assisted electrochemical oxidation, SEO) and electrochemical-based oxidation (EO) with Br-doped diamond (BDD) in conjunction with UV irradiation. The HCQ was entirely depleted from

aqueous solutions using EO with a BDD anode, independent of HCQ content, current intensity, or starting pH. The decay of HCQ was faster than the breakdown of the organic carbon (TOC) content, suggesting that the degrading of HCQ utilizing EO with the BDD anode comprises many stages that result in organic intermediate production that eventually mineralizes. Moreover, the results showed that in the early phases of HCQ breakdown, chloride (Cl^-) ions were released. Furthermore, organic nitrogen was mostly transformed to NO_3^- and NH_4^+ with minor quantities of volatile nitrogen species (NH_3 and NO_x).

4.2.2. Chloroquine Phosphate

MIL-88A(Fe) and perylene-34,910-tetracarboxylic diimide (PDINH) were used to make PDINH/MIL-88A(Fe) (PxMy) composites using a simple ball-milling method [114]. Under visible light from a low-power LED, the optimal P25M175 demonstrated that by activating peroxydisulfate (PDS), it is possible to degrade chloroquine phosphate (CQ) with remarkable efficiency, the plausible pathway is shown in Figure 5. The enhanced CQ photodegradation efficiency was assigned to the synergistic effects of PDS photocatalytic activation through direct electron transfer over the P25M175 and indirect electron transfer over the pristine MIL-88A. Both nonradical singlet oxygen ($^1O_2$) and active radicals (such radical $^{\bullet}SO_4^-$, radical $^{\bullet}OH$, radical $^{\bullet}O_2^-$, h^+) contributed to the CQ breakdown, according to results from electron spin resonance (ESR) measurements and capturing of active species experiments. On the basis of LC–MS analysis and DFT calculations, CQ breakdown routes and intermediate toxicity assessments were provided. P25M175 also exhibited high stability and reusability. The outcomes of this research shed light on the processes of organic contaminant breakdown using photocatalysis-activated SR-AOP on a Fe-MOF-based photocatalyst.

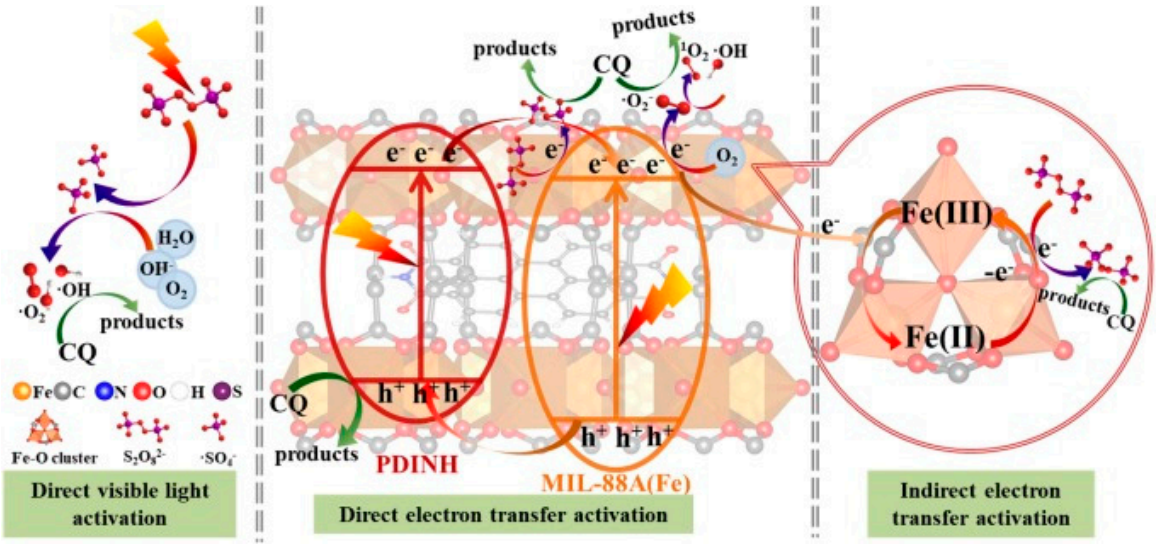

Figure 5. A possible pathway for photocatalysis-activated SR−AOP oxidation of CQ over P25M175 in the presence of LED visible light. Reprinted/adapted with permission from Ref. [114]. Copyright 2021 Elsevier.

5. Anti-Inflammatory Glucocorticoids

Glucocorticoids are commonly taken to reduce inflammation in long-term inflammatory illnesses such as rheumatoid arthritis, asthma, autoimmune diseases, and inflammatory bowel disease, all of which are linked to elevated inflammatory gene expression. They work by interacting with the glucocorticoid receptor (GR) [115].

5.1. Dexamethasone

Dexamethasone ((DXM), (IUPAC name: 8S,9R,10S,11S,13S,14S,16R,17R)-9-Fluoro-11,17-dihydroxy-17-(2-hydroxyacetyl)-10,13,16-trimethyl-6,7,8,9,10,11,12,13,14,15,16,17-

dodecahydro-3H-cyclopenta[a]phenanthren-3-one, molecular formula: $C_{22}H_{29}FO_5$) was shown to reduce 28-day death in patients hospitalized with COVID-19 who were getting either invasive mechanical ventilation or oxygen alone at the time of randomization, but not in those who did not receive any respiratory support [116]. Besides its effectiveness against COVID-19 and other diseases like cancer, dexamethasone has some bad effects on the environment and human health. When you take dexamethasone for a long time, you run the chance of developing additional adverse effects. Long-term use may result in thinning bones (osteoporosis), vision difficulties, and slowed development in children and teens [117]. So it is essential to derogate this drug properly.

The use of Ag/TiO_2-based nanomaterials as innovative photocatalysts applicable in the photodegradation of DXM in an aqueous environment was studied in [118]. Moreover, pure TiO_2 (70% anatase and 30% rutile) and Ag/TiO_2 characteristics and activities were examined. Both samples had nanoparticles that were almost spherical in shape with a little aggregation, according to the findings. Titanium dioxide's crystallinity is considerably affected by the coated silver, but not its structure. Under visible light irradiation, Ag/TiO_2 samples are also highly reactive. The major goal of this research is to see how operational circumstances affect DXM reaction kinetics and degrading efficiency. Various Ag/TiO_2 photocatalyst concentration ranges (0.75–2.5 g L^{-1}), H_2O_2 (10–20 mg L^{-1}), and initial DXM (5–30 mg L^{-1}) were used in the visible-light and UV irradiation photocatalyst studies. Temperature (30–80) and pH (3–11) were also studied. For a catalyst concentration of 1.5 g L^{-1}, a temperature of 35 °C, pH = 3, and an initial DXM concentration of 5 mg L^{-1}, the optimum photodegradation of DXM was achieved, resulting in degradation efficiency of 63.8% and 77.6%, for visible and UV irradiation, respectively. The degradation efficiency of visible and UV light irradiation was improved to 71.5% and 82.3%, respectively, by adding H_2O_2 to the optimum dose (15 mg L^{-1}).

The possibility of DXM breakdown utilizing photocatalytic methods involving ZrO_2 and WO_3 NPs was explored in [119]. Different factors, such as solution pH, DXM concentration, catalyst dose, contact duration, and irradiation sources were studied. The outcomes revealed that the best performance for both catalysts was obtained at pH 3. The best ZrO_2 and WO_3 catalyst dosages were 1500 and 500 mg L^{-1}, respectively. At a DXM concentration of 5 mg L^{-1}, the maximum breakdown was achieved. The examination of several irradiation sources revealed that the BLB/WO_3 method was able to remove DXM completely. Furthermore, Halogen/WO_3 in synthetic solutions was able to produce around 50% mineralization of DXM, the degradation mechanism is shown in Figure 6. In real hospital wastewater, the process performance and degree of DXM mineralization were also examined, and the results revealed that the real-world solution was less efficient than the synthetic solution. Furthermore, pseudo-first-order and second-order processes were used to evaluate the experimental kinetics data. The UV/TiO_2 photocatalytic system showed the greatest R^2 value of 0.99. DXM was fully destroyed using halogen/WO_3 in real hospital wastewater after a 100-min contact period.

In another study, da Silva et al. [120] found that in the presence of a petrochemical residue-supported photocatalyst, dexamethasone and guaifenesin were destroyed in a similar way under visible and UV light. Photochemical experiments were also conducted in the presence of commercial titania for comparison purposes (P25). In the dark and with LED irradiation, using cyclic voltammetry and differential pulse voltammetry, the supported photocatalyst photoelectrochemical behavior was investigated. The greatest drug degradation values were reported for guaifenesin under visible (45.2%) and UV (48.6%) radiation using the synthetic photocatalyst in this photodegradation research. The commercial P25 catalyst achieved 50.2 and 66.3% degradation under visible and UV radiation, respectively, under the same circumstances. The device may be sensitive to additional analytes present in these ambient samples, according to preliminary experiments using tap water samples.

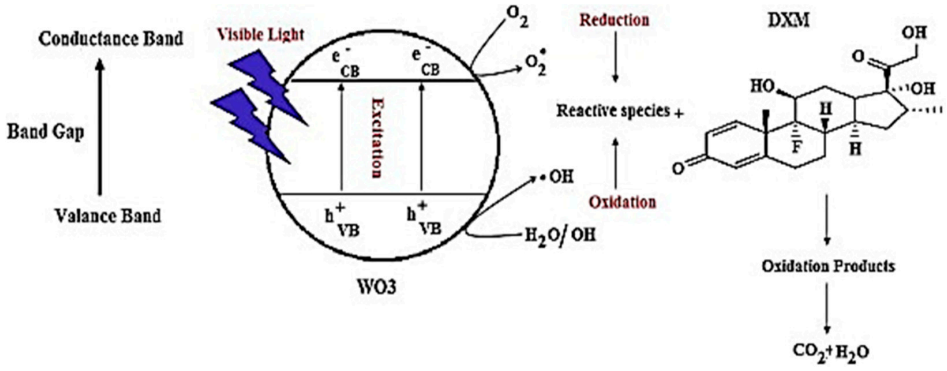

Figure 6. Photocatalytic-based degradation mechanism of DXM in the presence of WO_3 nanoparticles. Reprinted/adapted with permission from Ref. [119]. Copyright 2019 Elsevier.

5.2. Cortisone Acetate

A carbon source was utilized to make carbon-doped ceria (CeO_2) as a visible light photocatalyst [121]. It is known that CeO_2, especially in the form of nanomaterials, can act as an effective antioxidant for anti-inflammatory purposes [122]. To make a solid powder carbon-doped ceria material, saturated ceria NPs were heated at 300 °C for 4 h after being saturated with sucrose solution. Data from the characterization revealed that between the ceria nanocrystals is the place of formation of graphite-like particles. Furthermore, the produced sample's light absorption displayed a noticeable red-shift towards visible light. The obtained materials' photocatalytic activity was investigated under visible light radiation. The mechanism of cortisone acetate (IUPAC name: [2-[(8S,9S,10R,13S,14S,17R)-17-hydroxy-10,13-dimethyl-3,11-dioxo-1,2,6,7,8,9,12,14,15,16-decahydrocyclopenta[a]phenanthren-17-yl]-2-oxoethyl] acetate, molecular formula: $C_{23}H_{30}O_6$) breakdown in a slurry reactor is shown in Figure 7. Carbon-doped CeO_2 photocatalytic activity was 6.8 times greater than that of commercially accessible ceria. Furthermore, carbon-doped ceria was effectively reused three times in a row with minimal activity loss. Recently, Se nanoparticles have also been nominated as effective nanomaterials for anti-inflammatory purposes [123].

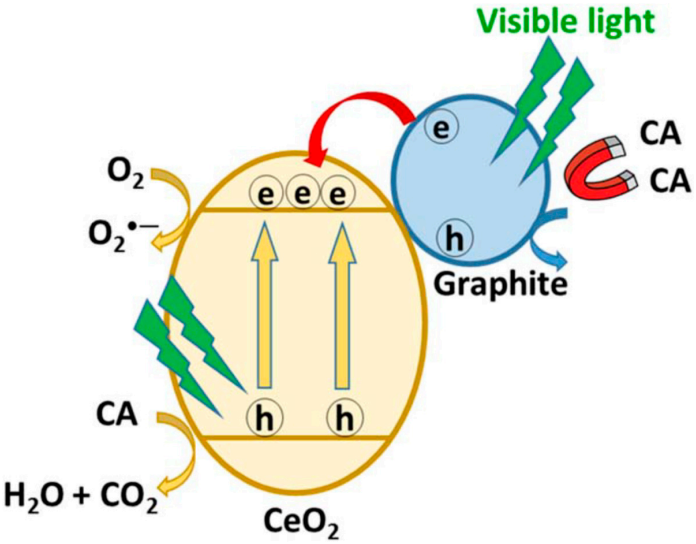

Figure 7. Photocatalytic degradation mechanism of cortisone acetate by using carbon-doped CeO_2 under visible light irradiation. Reprinted/adapted with permission from Ref. [121]. Copyright 2019 Institute of Physics.

6. Antihistamines

Antihistamines were evaluated in a mixture of human and monkey cells for their ability to suppress the coronavirus. Three of the medicines, diphenhydramine, hydroxyzine, and azelastine, had direct antiviral effects on the coronavirus, which were statistically significant [124]. However, antihistamines are weakly eliminated/degraded by the biological treatment methods used in wastewater treatment facilities, and as a result, they are routinely released into the aquatic environment with other pharmaceuticals [125].

Diphenhydramine

Antihistamines, such as diphenhydramine ((DP), IUPAC name: 2-(diphenylmethoxy)-N,N-dimethylethanamine, molecular formula: $C_{17}H_{21}NO$), are commonly used to treat allergies. They are also good for sleeplessness, cold symptoms, parkinsonian tremors, and nausea. They can be taken orally, injected into a vein, or muscle, or administered directly to the skin. The maximum impact usually occurs two hours after dosage, although it might continue up to seven hours [126]. As we said, it is also effective in the control of COVID-19. We will discuss its photocatalytic degradation in this part.

In an interesting work [127], natural dolomite, as a cheap and widely accessible natural material, was shown to be a promising heterogeneous photocatalyst for removing DP effectively from aqueous solutions when exposed to artificial sunlight. With dolomite as a catalyst, DP elimination of 65% and mineralization of 14% were obtained after 75 min of irradiation. Scavenger testing and electron spin resonance studies confirmed that the main reactive species involved in the degradation of DP were $^1O_2$, $^\bullet OH$, and $^\bullet O_2^-$ generated in the system of dolomite. To further explain the photocatalytic process, first-principle calculations were coupled with deoxygenation observations. After partial replacement of Mg^{2+} by Fe^{2+}, the dolomite transformed from an insulator to a semiconductor, implying that in photoreactions, natural dolomite might function as a semiconductor photocatalyst. Photo-excited holes and electrons split and move to the dolomite surface under irradiation, where they combine to produce reactive species, causing DP deterioration. The major degradation mechanisms of DP were found to include the aromatic ring hydroxylation and the alkylamine side chain's hydroxyl radical-mediated oxidation, according to product analyses.

The effectiveness of a novel TiO_2 catalyst (ECT) produced using an improved sol–gel technique for degradation of a significant pharmaceutical contaminant in water, DP was investigated by Pastrana-Martínez et al. [128]. The activity of DP is compared to P25, an Evonik Degussa Corporation benchmark catalyst, at various catalytic loadings (more than 2.00 g L^{-1}) and initial pH of solution (3.0–11.0). The outcomes demonstrate that the DP is significantly stable in non-catalytic environments. By selecting the right TiO_2 loading, full breakdown and significant mineralization (ca. 60–70%) may be accomplished in 60 min under NUV (near UV) to visible light irradiation (~50 mW cm^{-2}). For the catalyst loadings greater than 1.00 g L^{-1}, ECT has substantially greater activity than the benchmark catalyst, and the pseudo-first-order rate constant rose as the pH of the solution grew from 3.0 to 11.0. At pH 11, with ECT, the highest rate constant was obtained (173×10^{-3} min^{-1} vs. 116×10^{-3} min^{-1} for P25). To study the photocatalytic process as a diagnostic tool, scavenger agents were employed, and it was discovered that holes are active species that are important in the photocatalytic process and that ECT has an availability that is higher than P25 for producing highly active radicals like hydroperoxyl (HOO•) and hydroxyl (HO•).

In another research performed at laboratory as well as pilot plant scales [129], DP hydrochloride (DPH) degradation by TiO_2 as a photocatalyst was investigated using a variety of light sources, including black blue light (BLB), UVC, solar light radiation (CPCs, Compound Parabolic Concentrators) and simulated solar radiation (SB, Solarbox). Photolysis had a significant role in DPH degradation when exposed to UVC light (32.5% of DPH conversion), but was insignificant in all other situations, according to the findings. In the SB device, several concentrations of TiO_2 (0.05, 0.1, and 0.4 g L^{-1}) were utilized, with the

greatest results coming from the 0.4 g L^{-1}: DPH conversion of 35.7% after 1 h of irradiation. In all of the devices, a TiO_2 concentration of 0.4 g L^{-1} was utilized for comparison. After 60 min of irradiation with just TiO_2, the highest results were DPH degradation of 44.8% in BLB and mineralization of 9.0% in SB. The photocatalytic process is improved by the addition of H_2O_2, and the greatest outcomes were achieved when UVC was employed, with a DPH breakdown of 100% and TOC reduction of 28.6%. UVC with H_2O_2 produced the best results in terms of removal efficiencies to energy used (4492 mg DPH/kWh and 2246 ppm DPH/kWh), as well as the lowest prices (2.89×10^{-5} €/mg DPH and 5.79×10^{-5} €/ppm DPH, respectively). BLB has the highest efficiency in the range of 380–400 nm (the absorption range of TiO_2). UVC with hydrogen peroxide has the highest values (7.64 h^{-1} and 0.493 kJ^{-1}), while the kinetic constants referred to the accumulated energy (kJ^{-1}) or irradiation time (h^{-1}) were estimated. Finally, the effects of reaction intermediates and toxicity were determined, and a pathway for DPH photodegradation was proposed.

In another investigation [130], using a straightforward technique of mixing and sonication (to adjust the concentration of GO and the temperature of heat-treatment under nitrogen), various composites of GO and P25 (GOP) were produced. The samples were identified by differential thermogravimetric (DTG) and thermogravimetric (TG) techniques, UV–Vis and IR DRS, physical adsorption of nitrogen, SEM, and point of zero charge measurements (pH_{PZC}). The composites' shape, S_{BET}, and microporosity did not differ substantially from P25, however, the development of GO aggregates covered with P25 NPs resulted in an increase in mesoporosity and mesopore diameter. The creation of Ti-O-C bonds stabilized the aggregates, resulting in a reduction of the optical band gap in comparison to P25. GOP composites' surface chemistry changed with the amount of GO utilized, becoming more acidic as the amount of GO increased. Under NUV/Vis irradiation, the photocatalytic efficacy of DP pharmaceutical and MO dye degradation was investigated. For some GOP composites, the MO photodegradation's first-order rate constant rose four-fold with respect to P25 (from $k = 52 \times 10^{-3}$ to 207×10^{-3} min^{-1}). When DP was employed as the model pollutant, similar efficiencies were obtained (~54×10^{-3} min^{-1}). The composite with the greatest performance was one that contained 1.4 wt% GO and was heated for treatment at 200–300 °C. The enhanced ability was ascribed to the reduced GO throughout the heat treatment, as well as to the excellent contact between the carbon phases and TiO_2.

Utilizing clinoptilolite natural zeolite, TiO_2/Fe_2O_3 and ZnO/Fe_2O_3 photocatalysts were synthetized using impregnation and sol-gel techniques. The existence of Fe_2O_3, ZnO, TiO_2 (both anatase and rutile phases), and NPs on the clinoptilolite surface was confirmed by XRD, EDX, and FT-IR findings. The FE-SEM findings verified the ZnO/Fe_2O_3 and TiO_2/Fe_2O_3 deposition on the zeolite surface. ZnO/Fe_2O_3 and TiO_2/Fe_2O_3 had particle sizes of around 34 and 47 nm, respectively. The produced NPs had 0.06 molar ratios of Fe^{3+}/ZnO and Fe^{3+}/TiO_2 in ZnO/Fe_2O_3/Zeolite and TiO_2/Fe_2O_3/Zeolite, respectively, according to XRF findings. The ZnO/Fe_2O_3/Zeolite and TiO_2/Fe_2O_3/Zeolite surface area, according to BET results, was around 289 and 112 m^2 g^{-1}, respectively. Both ZnO/Fe_2O_3/Zeolite and TiO_2/Fe_2O_3/Zeolite have a good capacity of absorption in the range of visible light, according to UV-Vis DRS study. The impact of operational parameters such as contaminant concentration (1–100 mg L^{-1}), photocatalyst concentration (0.5–2 g L^{-1}), irradiation time (45–180 min), and pH (4–10) on the DP degradation performance of these two photocatalysts from polluted water was investigated in [131]. In comparison to TiO_2/Fe_2O_3/Zeolite, the photocatalytic tests indicated that ZnO/Fe_2O_3/Zeolite had a better capability in the degradation of DP. The efficiency of DP photodegradation with ZnO/Fe_2O_3/Zeolite (DP: 50 mg L^{-1}, irradiation time: 100 min, hydrogen peroxide: 50 mg L^{-1}, PH = 10, photocatalyst: 0.5 g L^{-1}) and TiO_2/Fe_2O_3/Zeolite (DP: 50 mg L^{-1}, time of irradiation: 120 min, hydrogen peroxide: 50 mg L^{-1}, pH = 5, photocatalyst: 0.5 g L^{-1}) was 95% and 80%, respectively.

7. H2 Blockers

H2 blockers are a class of drugs that work by lowering the amount of acid generated by the cells in the stomach lining. H2 blockers are also known as histamine H2-receptor antagonists. Famotidine, nizatidine, cimetidine, and ranitidine are examples of these drugs [132].

Famotidine

Famotidine (IUPAC name: 3-[({2-[(diaminomethylidene)amino]-1,3-thiazol-4-yl}methyl) sulfanyl]-N-sulfamoylpropanimidamide, molecular formula: $C_8H_{15}N_7O_2S_3$), when given to hospitalized patients at a high dosage with coronavirus, was shown to lower the rates of intubation and death, according to a new large-scale, retrospective clinical research. Famotidine was linked to improvements in mild to moderate symptoms including shortness of breath and cough in different patient-reported research. Photocatalytic degradation of this drug is important because of its widespread usage.

In a recent study [133], using Pluronic P123, Pluronic F127, CTAB, and Synperonic F108 as structure-directing agents, excellent 2-dimensional hexagonal ordered mesoporous TiO_2 with a large surface area and a well-crystallized framework structure was synthesized properly in a repeatable manner, and the nanostructured matrix that resulted was developed as TMP-123, TMF-127, TMC-016/TMC-036, and TMF-108, respectively. By adjusting the pore structure, all of these materials display large quantities of inherent defects, such as electrons trapped in oxygen vacancies and/or Ti^{3+} centers. These flaws facilitate the charge separation of photogenerated excitons, resulting in high photocatalytic activity for famotidine breakdown (P-25: DE_{100} = 120 min; TMP-123: DE_{100} = 75 min) and 4-chlorophenol (P-25: DE_{60} = 180 min; TMP-123: DE_{95} = 180 min) degradation. The mesoporous TiO_2's superior activity over the fumed TiO_2 (P-25) is attributed to: 1-Absorption of light that extends into the visible spectrum, 2-Charge-transfer resistance is low, and carrier density is high, and 3-inherent Ti^{3+} defects, as determined by UV-vis DRS, EPR, and photo-electrochemical experiments (Nyquist and Mott–Schottky).

Under visible light, photocatalytic degradation of Famotidine (FMT) by dye-sensitized TiO_2 was studied by M. Molla et al. [134]. At room 25 °C and at the natural pH value of the solution, photodegradation tests were carried out using dye-sensitized 20 mg of TiO_2 and 30 mL of initial concentration of FMT (2 and 5 mg/L) at varied time intervals. The photoactivity of TiO_2 was improved by dye-sensitization using 5 mg/L orange II (OII), bromophenol blue (BPB), acid red 88 (AR88), and rhodamine B (RhB) in the breakdown of FMT. The photocatalytic mechanism for the TiO_2 dye-sensitized Famotidine degradation under irradiation of visible light was found to be mostly ascribed to oxidation by $^{\bullet}O_2^-$ and h^+ radicals, with the $^{\bullet}OH$ radicals playing only a small part in the oxidation process. The kinetics of FMT photodegradation were obtained to obey pseudo-first-order kinetics and could be modeled using the Langmuir–Hinshelwood model.

Integrated photocatalytic adsorbents (IPCAs) composed of TiO_2 nanostructures and AC were developed utilizing an ultrasonic impregnation method. SEM and FT-IR spectroscopy were used to study the IPCAs, which were then used for the famotidine photodegradation as catalysts under irradiation from a 125 W Hg lamp with modest pressure. A pseudo-first-order kinetic method was developed to govern the degradation kinetics, with various increments in the process's apparent first-order rate constant produced by varied TiO_2 loadings. A modified Langmuir–Hinshelwood model (LH) can be used to explain the kinetic behavior. With a k_r and K_C of 0.237 mg L^{-1} min^{-1} and 0.0172 L$(mg)^{-1}$, respectively, the IPCA produced with a 10% TiO_2 to AC loading had the greatest rate constant. The LH model explains the influence of the IPCA's TiO_2 concentration on the deterioration rate by fitting the experimental data. Calcination (heat treatment) was also examined in the production of IPCA and its influence on photocatalytic and adsorption performance. This study [135] showed that combining TiO_2 with AC produces a promising material for use in organic pollutant degradation.

8. Anthelmintics

A medication used to cure parasitic worm infections in animals is known as an anthelmintic. This applies to both worms, that are round and flat, such as nematodes, as well as flatworms (flukes (trematodes) and tapeworms (cestodes)). Human tropical medicine and veterinary medicine both rely heavily on parasites [136,137].

Praziquantel

Praziquantel ((PZQ), IUPAC name: (RS)-2-(Cyclohexylcarbonyl)-1,2,3,6,7,11b-hexahydro-4H-pyrazino[2,1-a]isoquinolin-4-one, molecular formula: $C_{19}H_{24}N_2O_2$), also known as Biltricide, is a parasitic worm medicine used in mammals, birds, reptiles, amphibians, and fish to treat a variety of parasitic worm diseases. Schistosomiasis, clonorchiasis, tapeworm infections, opisthorchiasis, cysticercosis, hydatid disease, and other fluke diseases are all treated with this drug in humans [138]. This medication is indicated for the control and treatment of COVID-19 based on research in African communities [139] so its proper degradation is important.

The PZQ can be photodegraded by utilizing UV light irradiation, TiO_2 film, and H_2O_2 (as an agent for Fenton reaction) in an oxidative direct photolysis reaction, as schematically represented in Figure 8 [140]. The photodegradation with 185/254 nm wavelengths as major (UV-C) was found to have higher performance with a 3.13-min half-life in comparison to the degradation that did not take place at 365 nm (UV-A). H_2O_2 was added to increase the rate of photolytic breakdown of PZQ, resulting in two to three times greater rates of degradation. TiO_2 film was utilized as a catalyst in the photocatalytic breakdown. The photocatalytic tests using UV-C light ($k = 0.2390\ min^{-1}$) degraded 10 times quicker than those using UV-A light ($k = 0.0201\ min^{-1}$). When the findings of all the tests are compared, it can be determined that the UV-C/TiO_2/H_2O_2 procedure gave the maximum rate of degradation, with total PZQ degradation taking less than 7 min. All of the studies showed that PZQ degradation followed first-order kinetics. In the presence of methanol, photodegradation was prevented. Based on the outcomes of the LC tandem MS study, five degradation products (m/z 273, 269, 189, 147, 132) were presented, along with their degradation pathways and structural formulae. It is interesting to note that the TiO_2/graphene oxide heterojunctions also showed efficient solar light-induced photocatalytic activities against nematode worms [30].

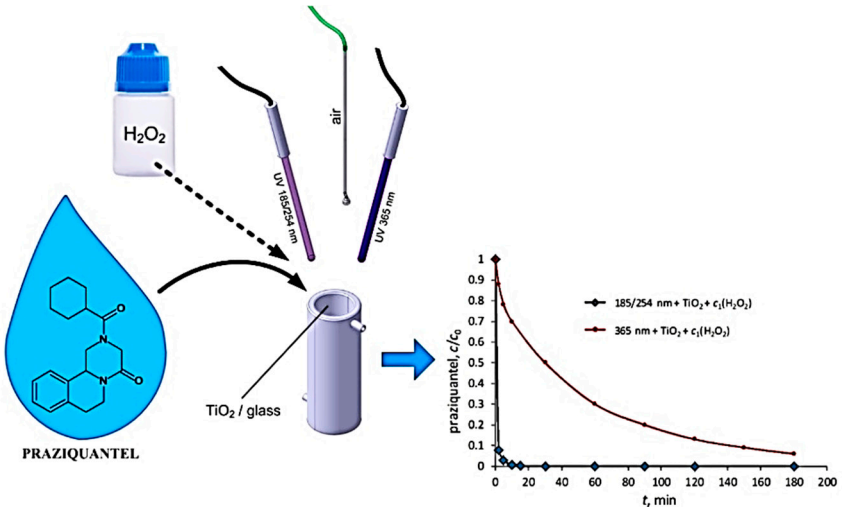

Figure 8. Schematic representation of photodegradation of PZQ using UV light, TiO_2 material, and H_2O_2 in oxidative photolysis processes. Reprinted/adapted with permission from Ref. [140]. Copyright 2017 Elsevier.

9. Antivirals

Antiviral medicines are a type of antiviral treatment that is used to combat viral infections. A wide-range antiviral is helpful against a large range of viruses, whereas most

antivirals target particular viruses. The medications can help to alleviate symptoms and decrease the duration of a viral illness. Antivirals also reduce the chances of contracting or transmitting viruses like herpes and HIV. Unlike lots of antibiotics, antiviral drugs do not kill their target pathogen; but they prevent it from growing [141].

9.1. Ivermectin

Using ivermectin (IUPAC name: 22,23-dihydroavermectin B_{1a} + 22,23-dihydroavermectin B_{1b}, molecular formula: $C_{48}H_{74}O_{14}$ + $C_{47}H_{72}O_{14}$), substantial reductions in COVID-19 fatalities are achievable, according to research with a moderate level of confidence. The use of ivermectin early in the clinical course may help to minimize the proportion of people who develop severe illness. Ivermectin is anticipated to have a big influence on the worldwide SARS-CoV-2 pandemic due to its apparent safety and inexpensive cost. Recent environmental risk evaluations of ivermectin have revealed the need for further knowledge on ivermectin's destiny in the environment. According to these findings, ivermectin binds firmly to soil and is photodegraded and biotransformed into less active molecules. Ivermectin, on the other hand, is very harmful to some aquatic species but is unlikely to partition into the aquatic environment. Based on these descriptions, its proper degradation is essential [142].

The forced degradation research and photocatalytic degradation routes of the two praziquantel ivermectin and anthelmintics in aqueous TiO_2 suspensions were examined and compared in [143]. When the TiO_2 content was raised from 0.25 to 2.00 g L^{-1}, the degradation activity for both substances rose, then stayed steady. The predicted k-values for IVE and PZQ were 0.36 h^{-1} to 0.64 h^{-1} and 0.29 h^{-1} to 0.47 h^{-1}, respectively. For 2.0 g L^{-1} of TiO_2, changing the pH from 3 to 9 had no notable effect on the degradation rate. After 5 h of irradiation, photodegradation was around 90% for both drugs. It was considerably hindered in the presence of iodide anion and isopropyl alcohol, indicating that OH radicals along with holes were involved in the breakdown of both anthelmintics. For IVE and PZQ, the contributions of OH radicals and holes were 92.1% and 93.2%, respectively. Three degradation intermediates were produced during the photocatalytic reaction of ivermectin, and two more were created through acidic and basic hydrolysis, degradation pathway is shown in Figure 9. Praziquantel was broken down into six degradation intermediates, four of which were produced by photocatalytic irradiation. UHPLC-MS/MS was used to identify the intermediates. For the detoxification of ivermectin and praziquantel, UV/TiO_2 photolysis has been proven to be an efficient advanced oxidation technique. It is interesting to note that the TiO_2-based materials with improved photocatalytic efficiency (e.g., by heterojunction formation on graphene surfaces) can also contribute to the degradation and inactivation of viruses themselves (see, for example, [28]).

In another investigation, Bosco et al. [144] looked at how photo-Fenton ($Fe^{2+}/H_2O_2/UV$) and Fenton (Fe^{2+}/H_2O_2) methods degraded ivermectin as well as how they removed acute toxicity (using Daphnia similis). The concentrations of H_2O_2 and Fe^{2+} were 0.5 to 10.0 mmol L^{-1} and 0.25 to 1.0 mmol L^{-1}, respectively. It was able to achieve 90% degrading efficiency with Fenton's reagent in 600 s, whereas the photo-Fenton achieved 99% in the same amount of time. Both methods had greater rates of breakdown in the first minute, with the toxicity decreasing as the time of the reaction progressed. The photo-Fenton method proved more effectivity in lowering drug concentrations and toxicity in solutions.

9.2. Acyclovir

Aciclovir ((ACV), IUPAC name: 2-Amino-1,9-dihydro-9-((2-hydroxyethoxy)methyl)-3H-purin-6-one, molecular formula: $C_8H_{11}N_5O_3$) is an antiviral medicine commonly known as acyclovir. Herpes simplex virus infections, chickenpox, and shingles are the most common conditions treated with it. Other applications include preventing CMV infections after transplantation and severe Epstein–Barr virus infection sequelae [145,146]. Because of its antiviral properties, acyclovir has been prescribed for the control of COVID-19. Due to inadequate biological treatments in wastewater treatment plants, ACV was frequently

discovered in natural water in quantities in the range of ng L^{-1} to μg L^{-1}. The methods for degradation of this drug have been discussed in the following.

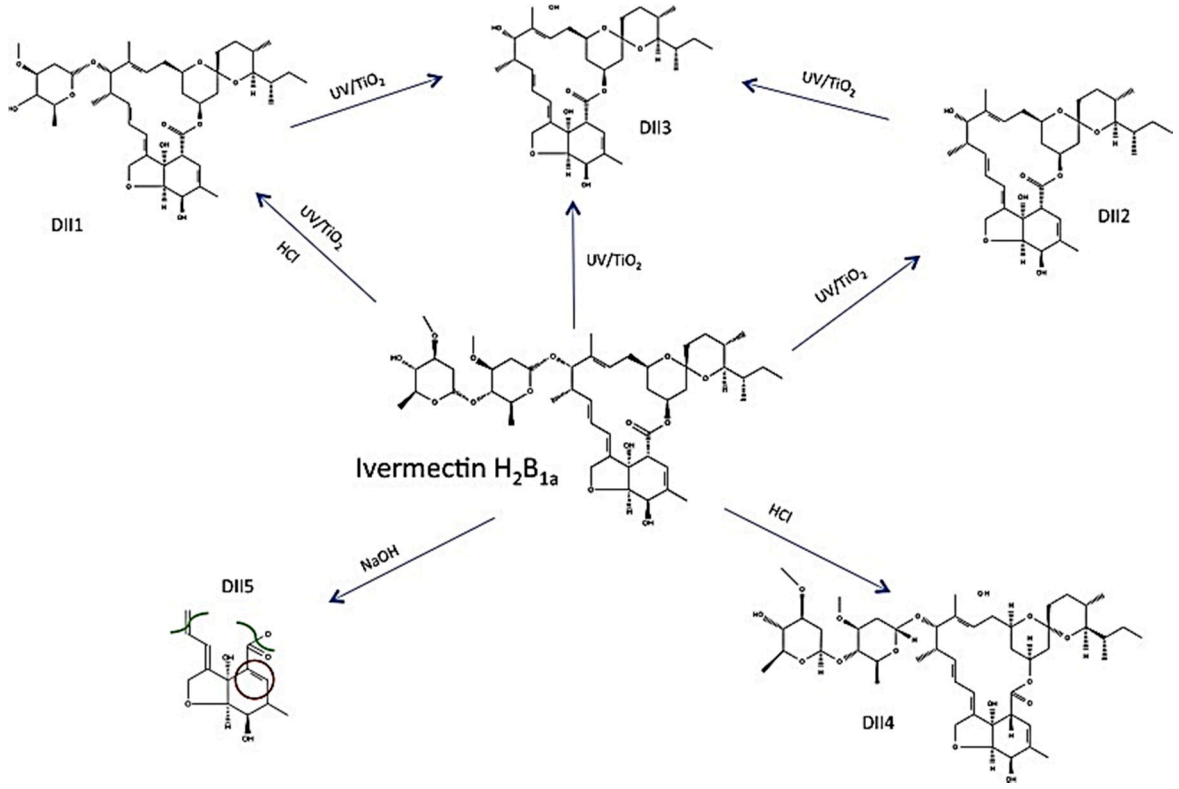

Figure 9. Ivermectin's proposed degradation route. Reprinted/adapted with permission from Ref. [143]. Copyright 2016 Elsevier.

In a photoreactor with a microcapillary film (MCF) array, the photochemical and ecotoxicological destiny of ACV was studied by direct photolysis of UV_{254} and in the involvement of OH radicals (UV_{254}/H_2O_2 condition), which gave ultrafast and precise kinetics of photochemical reactions [147]. The UVC photodegradation of ACV was shown to be unaffected by pH varying from 4.5 to 8.0, implying an autophotocatalytic mechanism. The production of a photochemical intermediate was one of the hypothesized mechanisms (ϕ_{ACV} = (1.62 ± 0.07) × 10^{-3} mol ein^{-1}), which reacted more with ACV to produce by-products (k' = (5.64 ± 0.03) × 10^{-3} M^{-1} s^{-1}). The production of hydroxyl radicals during ACV photolysis in the vicinity of H_2O_2 increased the elimination of ACV. For ACV reaction, the kinetic constant ($k_{OH/ACV}$) with OH radicals calculated using the kinetic modeling technique was (1.23 ± 0.07) × 10^9 M^{-1} s^{-1}, while the kinetic constant derived using the method of competition kinetics was (2.30 ± 0.11) × 10^9 M^{-1} s^{-1}. The mixture of treated aqueous has severe and long-term effects on several living species (*Raphidocelis subcapitata, Vibrio fischeri, and D. magna*) indicating that the catalysts treated with UV_{254}/H_2O_2 were substantially less hazardous than those obtained after UV_{254} treatment. This finding shows that adding a small amount of H_2O_2 (30–150 mg L^{-1}) would be a beneficial technique for lowering the ecotoxicity of UV_{254}/H_2O_2-based methods for water treatment.

The breakdown and mineralization of the antiviral medication acyclovir were tried utilizing heterogeneous photocatalytic technology, and it was found that the highly reactive •OH was the main cause of ACV degradation [148]. As a result, frontier electron densities were measured in order to predict probable starting locations during the photocatalytic breakdown, and the outcomes revealed that •OH additions at C8 and C5, as well as abstraction of H at C15, were the three most common breakdown paths for •OH initiating ACV breakdown. Moreover, the quantum chemical calculations method was used to study

the detailed mechanisms of degradation by identifying six major products through a series of experiments using HPLC/MS/MS, and the probability of three essential compounds' formation was evaluated to further verify the mechanism of photocatalytic degradation. Furthermore, related kinetic models were presented to investigate ACV removal and the production of one major product—guanine—over time profiles in order to double-check the hypothesized degradation process. Ultimately, the findings of the potential risk assessment revealed that when total organic carbon dropped, aquatic toxicities at three trophic levels quickly rose, then reduced.

The photodegradation of ACV, zidovudine, and lamivudine, which are antiviral medicines, in freshwater, clean water, and seawater in the presence of artificial sunlight was examined by Zhou et al. [149]. Zidovudine was simply changed by direct photolysis, but ACV and lamivudine were mostly transformed via indirect photolysis, according to the findings. In freshwater, they discovered that nitrate increased photodegradation, bicarbonate speeded up photodegradation of ACV, and dissolved organic matter (DOM) speeded up ACV photolysis and lamivudine. Cl^-, Br^-, and ionic strength had no effect on acyclovir photolysis in saltwater; however, Cl^- and Br^- hindered zidovudine photolysis, whereas Br^-, Cl^-, and ionic strength increased lamivudine photolysis. Second-order reaction rate constants with $^1O_2$ (k_{1O2}) and radical $^\bullet$OH (k_{OH}) were also determined for the three antiviral medicines.

In another investigation, Jia et al. [150] used photochemical tests using a Xe lamp that mimicked sunlight irradiation. For mechanism studies, isopropanol was employed as a radical trapping agent, and the toxic effects of ACV photoproducts were assessed using the acute toxicity assay of Photobacterium phosphoreum T_3 spp. The outcomes showed that the ACV photodegradation followed pseudo-first-order law kinetics and that the rate of ACV elimination enhanced when the pH was raised from 5 to 10. The photochemical reaction route shown by HPLC–MS/MS demonstrated that $^\bullet$OH may attack the C–C and C–N bonds of ACV, resulting in hydroxyl substitution products being the majority of the photoproducts. The intermediate photoproducts were more hazardous than the parent ACV during photodegradation, with the maximum toxicity impact occurring after 6 h.

9.3. Lopinavir/Ritonavir

Lopinavir/ritonavir ((LPV/RTV), IUPAC name: (2S)-N-[(2S,4S,5S)-5-[[2-(2,6-dimethylphenoxy)acetyl]amino]-4-hydroxy-1,6-diphenylhexan-2-yl]-3-methyl-2-(2-oxo-1,3-diazinan-1-yl)butanamide/ 1,3-thiazol-5-ylmethyl N-[(2S,3S,5S)-3-hydroxy-5-[[(2S)-3-methyl-2-[[methyl-[(2-propan-2-yl-1,3-thiazol-4-yl) methyl] carbamoyl] amino] butanoyl] amino]-1,6-diphenylhexan-2-yl] carbamate, molecular formula: C37H48N4O5/C37H48N6O5S2) is an antiretroviral drug used to cure and prevent HIV/AIDS. It is offered under the trade name Kaletra [151]. Based on in vitro activity, observational studies, and preclinical studies, lopinavir–ritonavir has been recommended as a therapy for COVID-19. However, lopinavir–ritonavir did not reduce 28-day mortality, the risk of invasive mechanical ventilation, hospital stay length, or death in COVID-19 hospitalized patients. The use of lopinavir–ritonavir in the therapy of COVID-19 hospitalized patients is not supported by these data [152]. Therefore, the degradation of this drug because of its environmental effects is important.

A validated stability-indicating LC-PDA technique was established to evaluate the breakdown behavior of Lopinavir, under hydrolysis (acid, basic, and neutral), oxidation, heat, and UV conditions [153]. Decomposition routes were postulated and LC-MS/MS analysis of degradation products was performed. Due to the existence of carbamate and urea linkages, which were sensitive to hydrolysis, the medication was shown to be destroyed significantly in all circumstances except oxidation. The drug's photochemical stability was further investigated by subjecting the 100 µg/mL solution to UV light for 7 days in a UV chamber or 200 Wh/m^2 in a photostability chamber. For the HPLC research, the resulting solution was diluted to 100 µg/mL, then 10 µL of it was poured into the apparatus, and to test the sample's stability, chromatograms were taken.

The invention and thorough confirmation of a stability-indicating HPLC technique for quantifying RTV and LPV in soft gelatin capsules is described in [154]. Isocratic elution with a LiChrospher® 100 RP-18 (250 mm × 4.6 mm, 5 µm, Merck) column is utilized in this technique. The mobile phase was a 53:37:10 ($v/v/v$) combination of acetonitrile, water, and methanol injected at a flow rate of 1.0 mL min^{-1}. A photodiode array sensor was employed to detect UV at 210 nm. The stressed samples of RTV and LPV were studied using the suggested technique after being subjected to thermal, oxidative stress, hydrolytic, and photolytic conditions. Within a range of 10–90 µg mL^{-1} for the RTV and 40–360 µg mL^{-1} for the LPV (with $r > 0.999$ for both drugs), the response was linear.

9.4. Favipiravir

Favipiravir (IUPAC name: 6-fluoro-3-hydroxypyrazine-2-carboxamide, molecular formula: $C_5H_4FN_3O_2$), an orally given medication with an action mechanism similar to remdesivir, has less evidence to support its usage, although it is appearing as a viable option in mild to moderate instances. The first findings from the first Indian research with this medication were promising, with a minor but substantial reduction in time to clinical recovery and a two-day decrease in viral shedding time [155]. Because of the wide use of the drug, its degradation has begun to be seen as an important issue.

The oxidative breakdown of the pyrazine antiviral medicines (T-1105) and favipiravir (T-705) using the electrogenerated superoxide radical anion ($^{\bullet}O_2^-$) was investigated by using electrochemical-based analyses and DFT calculations [156]. Antiviral RNA nucleobase analog T-1105 and T-705 target the RNA-dependent polymerase chain and stop it specifically. They might be a medication candidate for a variety of viral diseases, including COVID-19. During proton-coupled electron transfer (PCET), the pyrazine moiety was degraded by $^{\bullet}O_2^-$. The findings demonstrated that its active form, pyrazine-ribofuranosyl-5′-triphosphate, was rapidly oxidized by highly produced $^{\bullet}O_2^-$ in inflamed organs via the immune system's PCET process. This mechanistic study suggests that by modifying the pyrazine structure to regulate the PCET, oxidative breakdown of pyrazine derivatives can be avoided.

9.5. Nitazoxanide

Nitazoxanide (IUPAC name: [2-[(5-Nitro-1,3-thiazol-2-yl)carbamoyl]phenyl]ethanoate, molecular formula: $C_{12}H_9N_3O_5S$), marketed under the trade name Alinia among others, is a wide antiviral and antiparasitic agent used in medication to cure protozoal, helminthic, and viral infections [141,157,158]. The use of nitazoxanide against the coronavirus has already shown positive results in vitro [159]. Based on broadcasting these results, usage of the drug rose and its degradation became a concern.

Malesuik et al. [160] used a stability-indicating liquid chromatographic technique in order to analyze the deteriorated samples. In quartz cells, the breakdown was conducted in acetonitrile using coated pills or powdered oral suspension under UVC light at 254 nm. The kinetic parameters, including rate constants, order of reaction, half-life ($t_{1/2}$), and the time when 90% of the drug's initial concentration was remaining, were characterized. Under the experimental circumstances used, the photodegradation of nitazoxanide in a solution of acetonitrile for both pharmaceutical formulations is zero-order. The results show that the chromatographic approach for measuring nitazoxanide kinetics in the presence of its breakdown products is accurate. The photolability of the medication in solution is revealed in this investigation.

9.6. Remdesivir

Remdesivir (IUPAC name: (2S)-2-{(2R,3S,4R,5R)-[5-(4-Aminopyrrolo[2,1-f] [1,2,4]triazin-7-yl)-5-cyano-3,4-dihydroxy-tetrahydro-furan-2-ylmethoxy]phenoxy-(S)-phosphorylamino} propionic acid 2-ethyl-butyl ester, molecular formula: $C_{27}H_{35}N_6O_8P$), commonly known as Veklury, is an antiviral medication with a wide range of uses. It is administered as a venous injection. During the coronavirus pandemic, Remdesivir was allowed for emergency

use in over 50 nations. Remdesivir was first made to help people with hepatitis C, then evaluated for Ebola and Marburg virus infections before being investigated as a COVID-19 post-infection medication [161,162].

Hamdy et al. [163] presented a chromatographic separation technique on a C18 column (250 × 4.6 mm and thickness of 5 µm) with detection from two sources: fluorescence at $\lambda_{ex/em}$ 245/390 nm and diode array at a wavelength of 240 nm. The acetonitrile and DI water (acidified with H_3PO_4 at pH = 4) were eluted isocratically at a volume ratio of 55:45. For HPLC-diode array sensing, the linearity range was from 0.1 to 15 µg/mL, while it was observed from 0.05 to 15 µg/mL for detection via fluorimetry. The RDV was found to be destroyed by acidic, alkaline, heat, neutral hydrolysis, photolytic, and oxidative stress conditions, according to the International Conference on Harmonization standards.

Rem's photostability was tested in the presence of UV light in [164]. The solvent combination for the preparation of the samples was ACN:HPLC water (1:1) based on the HPLC method for Rem. In the scintillation vials, the Rem stock produced in NMP was diluted by ACN:HPLC water (1:1) to obtain a concentration of 50 µg/mL. The vials were inserted into a UV light chamber to assess Rem's photodegradation. The samples were taken at 0-, 1-, 3-, and 5-day intervals, and the drug concentration was determined by HPLC.

10. Outlook and Conclusions

The pandemic of COVID-19 has become one of the most serious global threats. Many medicines, including painkillers, mucolytics, and anti-biotic/viral/inflammatory drugs, have been prescribed to control symptoms caused by this disease. These medications have detrimental effects on the health and ecology of microorganisms, plants, animals, and humans because they pollute terrestrial and aquatic ecosystems by entering surface waters through pharmaceutical manufacture and frequently excreting trace amounts of waste after human use. Residual medicines in water have the ability to damage aquatic species, useful and required microorganisms, as well as alter their food chain and breeding cycle. As a result, appropriate degradation of these widely used medications is critical. In addition, more suitable social responsibilities for prescribing effective antibiotics/antiviral drugs and management of unused and/or ineffective drugs should be considered, announced, and implemented. Direct discharge of pharmaceutical wastes into the living environment and surface water must be prevented. For a long-term program, the public health level of the communities should be significantly enhanced by impressive instructions/advertisements to reduce the number of patients requiring drugs for the treatment. Meantime, photocatalytic degradation of pharmaceutical wastes within the treatment site of the hospitals and drug factories can be considered one of the effective methods for reducing the irreversible side effects of the wastes on the environment. In this review, we showed that analgesics, mucolytics, antibiotics, anti-inflammatory glucocorticoids, antihistamines, H2 blockers, anthelmintics, and finally antivirals (as being widely used in controlling/treating the coronavirus) can be environment-friendlily degraded by suitable catalysts, for saving the unique ecosystem of our planet. Therefore, it can excite more attention regarding the further controlled/limited use of commercial pharmaceutical products by medical treatment teams in hospitals and by people themselves.

Author Contributions: Conceptualization, O.A.; methodology, M.E. and O.A.; validation, M.E. and O.A.; investigation, M.E. and O.A.; resources, O.A.; writing—original draft preparation, M.E. and O.A.; writing—review and editing, O.A.; visualization, O.A.; supervision, O.A.; project administration, O.A. All authors have read and agreed to the published version of the manuscript.

Funding: This research received no external funding.

Conflicts of Interest: The authors declare no conflict of interest.

References

1. Finnerup, N.B. Nonnarcotic Methods of Pain Management. *N. Engl. J. Med.* **2019**, *18*, 61. [CrossRef] [PubMed]
2. Bakshani, C.R.; Morales-Garcia, A.L.; Althaus, M.; Wilcox, M.D.; Pearson, J.P.; Bythell, J.C.; Burgess, J.G. Evolutionary Conservation of the Antimicrobial Function of Mucus: A First Defence against Infection. *NPJ Biofilms Microb.* **2018**, *4*, 1–12. [CrossRef] [PubMed]
3. Kapoor, G.; Saigal, S.; Elongavan, A. Action and Resistance Mechanisms of Antibiotics: A Guide for Clinicians. *J. Anaesthesiol. Clin. Pharmacol.* **2017**, *33*, 300–305. [CrossRef] [PubMed]
4. C Reygaert, W. An Overview of the Antimicrobial Resistance Mechanisms of Bacteria. *AIMS Microbiol.* **2018**, *4*, 482–501. [CrossRef]
5. Ahmed, M.H.; Hassan, A. Dexamethasone for the Treatment of Coronavirus Disease (COVID-19): A Review. *SN Compr. Clin. Med.* **2020**, *2*, 2637–2646. [CrossRef]
6. Villoutreix, B.O.; Krishnamoorthy, R.; Tamouza, R.; Leboyer, M.; Beaune, P. Chemoinformatic Analysis of Psychotropic and Antihistaminic Drugs in the Light of Experimental Anti-Sars-Cov-2 Activities. *Adv. Appl. Bioinform. Chem.* **2021**, *14*, 71–85. [CrossRef]
7. Reznikov, L.R.; Norris, M.H.; Vashisht, R.; Bluhm, A.P.; Li, D.; Liao, Y.S.J.; Brown, A.; Butte, A.J.; Ostrov, D.A. Identification of Antiviral Antihistamines for COVID-19 Repurposing. *Biochem. Biophys. Res. Commun.* **2021**, *538*, 173–179. [CrossRef]
8. Spiro, H.M. H_2-Blockers. *J. Clin. Gastroenterol.* **1983**, *5*, 143–148. [CrossRef]
9. Kausar, S.; Said Khan, F.; Ishaq Mujeeb Ur Rehman, M.; Akram, M.; Riaz, M.; Rasool, G.; Hamid Khan, A.; Saleem, I.; Shamim, S.; Malik, A. A Review: Mechanism of Action of Antiviral Drugs. *Int. J. Immunopathol. Pharmacol.* **2021**, *35*, 20587384211002621. [CrossRef]
10. Zhou, L.J.; Li, J.; Zhang, Y.; Kong, L.; Jin, M.; Yang, X.; Wu, Q.L. Trends in the Occurrence and Risk Assessment of Antibiotics in Shallow Lakes in the Lower-Middle Reaches of the Yangtze River Basin, China. *Ecotoxicol. Environ. Saf.* **2019**, *183*, 109511. [CrossRef]
11. Chen, X.; Lei, L.; Liu, S.; Han, J.; Li, R.; Men, J.; Li, L.; Wei, L.; Sheng, Y.; Yang, L.; et al. Occurrence and Risk Assessment of Pharmaceuticals and Personal Care Products (PPCPs) against COVID-19 in Lakes and WWTP-River-Estuary System in Wuhan, China. *Sci. Total Environ.* **2021**, *792*, 148352. [CrossRef] [PubMed]
12. Morales-Paredes, C.A.; Rodríguez-Díaz, J.M.; Boluda-Botella, N. Pharmaceutical Compounds Used in the COVID-19 Pandemic: A Review of Their Presence in Water and Treatment Techniques for Their Elimination. *Sci. Total Environ.* **2022**, *2021*, 152691. [CrossRef] [PubMed]
13. Boxall, A.B.A. The Environmental Side Effects of Medication. *EMBO Rep.* **2004**, *5*, 1110–1116. [CrossRef]
14. Melander, R.J.; Melander, C. The Challenge of Overcoming Antibiotic Resistance: An Adjuvant Approach? *ACS Infect. Dis.* **2017**, *3*, 559–563. [CrossRef] [PubMed]
15. Kuroda, K.; Li, C.; Dhangar, K.; Kumar, M. Predicted Occurrence, Ecotoxicological Risk and Environmentally Acquired Resistance of Antiviral Drugs Associated with COVID-19 in Environmental Waters. *Sci. Total Environ.* **2021**, *776*, 145740. [CrossRef]
16. Holmes, E.C.; Hurt, A.C.; Dobbie, Z.; Clinch, B.; Oxford, J.S.; Piedra, P.A. Understanding the Impact of Resistance to Influenza Antivirals. *Clin. Microbiol. Rev.* **2021**, *34*, e00224-20. [CrossRef]
17. Afshari, R.; Akhavan, O.; Hamblin, M.R.; Varma, R.S. Review of Oxygenation with Nanobubbles: Possible Treatment for Hypoxic COVID-19 Patients. *ACS Appl. Nano. Mater.* **2021**, *4*, 11386–11412. [CrossRef]
18. Rodríguez, S.M.; Richter, C.; Gálvez, J.B.; Vincent, M. Photocatalytic Degradation of Industrial Residual Waters. *Sol. Energy* **1996**, *56*, 401–410. [CrossRef]
19. Gümüş, D.; Akbal, F. Photocatalytic Degradation of Textile Dye and Wastewater. *Water. Air. Soil Pollut.* **2011**, *216*, 117–124. [CrossRef]
20. Khan, S.H.; Pathak, B. Zinc Oxide Based Photocatalytic Degradation of Persistent Pesticides: A Comprehensive Review. *Environ. Nanotechnol. Monit. Manag.* **2020**, *13*, 100290. [CrossRef]
21. Fakhri, A.; Naji, M. Degradation Photocatalysis of Tetrodotoxin as a Poison by Gold Doped PdO Nanoparticles Supported on Reduced Graphene Oxide Nanocomposites and Evaluation of Its Antibacterial Activity. *J. Photochem. Photobiol. Biol.* **2017**, *167*, 58–63. [CrossRef] [PubMed]
22. Ziolli, R.L.; Jardim, W.F. Photocatalytic Decomposition of Seawater-Soluble Crude-Oil Fractions Using High Surface Area Colloid Nanoparticles of TiO_2. *J. Photochem. Photobiol. Chem.* **2002**, *147*, 205–212. [CrossRef]
23. Rachna; Rani, M.; Shanker, U. Degradation of Tricyclic Polyaromatic Hydrocarbons in Water, Soil and River Sediment with a Novel TiO_2 Based Heterogeneous Nanocomposite. *J. Environ. Manag.* **2019**, *248*, 109340. [CrossRef] [PubMed]
24. Meidanchi, A.; Akhavan, O.; Khoei, S.; Shokri, A.A.; Hajikarimi, Z.; Khansari, N. ZnFe2O4 Nanoparticles as Radiosensitizers in Radiotherapy of Human Prostate Cancer Cells. *Mater. Sci. Eng.* **2015**, *46*, 394–399. [CrossRef] [PubMed]
25. Akhavan, O.; Ghaderi, E. Escherichia coli bacteria reduce graphene oxide to bactericidal graphene in a self-limiting manner. *Carbon* **2012**, *50*, 1853–1860. [CrossRef]
26. Ren, S.; Boo, C.; Guo, N.; Wang, S.; Elimelech, M.; Wang, Y. Photocatalytic Reactive Ultrafiltration Membrane for Removal of Antibiotic Resistant Bacteria and Antibiotic Resistance Genes from Wastewater Effluent. *Environ. Sci. Technol.* **2018**, *52*, 8666–8673. [CrossRef]
27. Mali, S.C.; Dhaka, A.; Githala, C.K.; Trivedi, R. Green Synthesis of Copper Nanoparticles Using Celastrus Paniculatus Willd. Leaf Extract and Their Photocatalytic and Antifungal Properties. *Biotechnol. Rep.* **2020**, *27*, e00518. [CrossRef]

28. Akhavan, O.; Choobtashani, M.; Ghaderi, E. Protein Degradation and RNA Efflux of Viruses Photocatalyzed by Graphene-Tungsten Oxide Composite under Visible Light Irradiation. *J. Phys. Chem.* **2012**, *116*, 9653–9659. [CrossRef]
29. Ebrahimi, M.; Asadi, M.; Akhavan, O. Graphene-Based Nanomaterials in Fighting the Most Challenging Viruses and Immunogenic Disorders. *ACS Biomater. Sci. Eng.* **2022**, *8*, 54–81. [CrossRef]
30. Akhavan, O.; Ghaderi, E.; Rahimi, K. Adverse Effects of Graphene Incorporated in TiO_2 Photocatalyst on Minuscule Animals under Solar Light Irradiation. *J. Mater. Chem.* **2012**, *22*, 23260–23266. [CrossRef]
31. Sarkar, S.; Chakraborty, S.; Bhattacharjee, C. Photocatalytic Degradation of Pharmaceutical Wastes by Alginate Supported TiO_2 Nanoparticles in Packed Bed Photo Reactor (PBPR). *Ecotoxicol. Environ. Saf.* **2015**, *2*, 35. [CrossRef] [PubMed]
32. Jiang, L.; Zhou, S.; Yang, J.; Wang, H.; Yu, H.; Chen, H.; Zhao, Y.; Yuan, X.; Chu, W.; Li, H. Near-Infrared Light Responsive TiO_2 for Efficient Solar Energy Utilization. *Adv. Funct. Mater.* **2022**, *32*, 2108977. [CrossRef]
33. Hunge, Y.M.; Yadav, A.A.; Khan, S.; Takagi, K.; Suzuki, N.; Teshima, K.; Terashima, C.; Fujishima, A. Photocatalytic Degradation of Bisphenol A Using Titanium Dioxide@nanodiamond Composites under UV Light Illumination. *J. Colloid Interf. Sci.* **2021**, *582*, 1058–1066. [CrossRef] [PubMed]
34. Hunge, Y.M.; Yadav, A.A.; Kang, S.W.; Kim, H. Photocatalytic Degradation of Tetracycline Antibiotics Using Hydrothermally Synthesized Two-Dimensional Molybdenum Disulfide/Titanium Dioxide Composites. *J. Colloid Interf. Sci.* **2022**, *606*, 454–463. [CrossRef]
35. Varma, K.S.; Tayade, R.J.; Shah, K.J.; Joshi, P.A.; Shukla, A.D.; Gandhi, V.G. Photocatalytic Degradation of Pharmaceutical and Pesticide Compounds (PPCs) Using Doped TiO_2 Nanomaterials: A Review. *Water Energ. Nexus* **2020**, *3*, 46–61. [CrossRef]
36. Rokhsat, E.; Akhavan, O. Improving the Photocatalytic Activity of Graphene Oxide/ZnO Nanorod Films by UV Irradiation. *Appl. Surf. Sci.* **2016**, *371*, 590–595. [CrossRef]
37. Akhavan, O. Thickness Dependent Activity of Nanostructured TiO_2/α- Fe_2O_3 Photocatalyst Thin Films. *Appl. Surf. Sci.* **2010**, *257*, 1724–1728. [CrossRef]
38. Begum, S.; Ahmaruzzaman, M. Biogenic Synthesis of SnO_2/Activated Carbon Nanocomposite and Its Application as Photocatalyst in the Degradation of Naproxen. *Appl. Surf. Sci.* **2018**, *449*, 780–789. [CrossRef]
39. Akhavan, O.; Ghaderi, E. Cu and CuO Nanoparticles Immobilized by Silica Thin Films as Antibacterial Materials and Photocatalysts. *Surf. Coat. Technol.* **2010**, *205*, 219–223. [CrossRef]
40. Chaudhari, S.M.; Gonsalves, O.S.; Nemade, P.R. Enhanced Photocatalytic Degradation of Diclofenac with Agl/CeO_2: A Comparison with Mn, Cu and Ag-Doped CeO_2. *Mater. Res. Bull.* **2021**, *143*, 111463. [CrossRef]
41. Zirak, M.; Akhavan, O.; Moradlou, O.; Nien, Y.T.; Moshfegh, A.Z. Vertically Aligned ZnO@CdS Nanorod Heterostructures for Visible Light Photoinactivation of Bacteria. *J. Alloys Compd.* **2014**, *590*, 507–513. [CrossRef]
42. Czech, B.; Zygmunt, P.; Kadirova, Z.C.; Yubuta, K.; Hojamberdiev, M. Effective Photocatalytic Removal of Selected Pharmaceuticals and Personal Care Products by Elsmoreite/Tungsten Oxide@ZnS Photocatalyst. *J. Environ. Manag.* **2020**, *270*, 110870. [CrossRef]
43. Yadav, A.A.; Hunge, Y.M.; Kang, S.W. Porous Nanoplate-like Tungsten Trioxide/Reduced Graphene Oxide Catalyst for Sonocatalytic Degradation and Photocatalytic Hydrogen Production. *Surf. Interfaces* **2021**, *24*, 101075. [CrossRef]
44. Wang, Y.; Niu, J.; Zhang, Z.; Long, X. Sono-Photocatalytic Degradation of Organic Pollutants in Water. *Prog. Chem.* **2008**, *20*, 1621–1627. [CrossRef]
45. Akhavan, O. Lasting Antibacterial Activities of Ag-TiO_2/Ag/a-TiO_2 Nanocomposite Thin Film Photocatalysts under Solar Light Irradiation. *J. Colloid Interf. Sci.* **2009**, *336*, 117–124. [CrossRef]
46. Jiang, L.; Yang, J.; Zhou, S.; Yu, H.; Liang, J.; Chu, W.; Li, H.; Wang, H.; Wu, Z.; Yuan, X. Strategies to Extend Near-Infrared Light Harvest of Polymer Carbon Nitride Photocatalysts. *Coord. Chem. Rev.* **2021**, *439*, 213947. [CrossRef]
47. Moma, J.; Baloyi, J. Modified Titanium Dioxide for Photocatalytic Applications. In *Photocatalysts-Applications and Attributes*; BahadarKhab, S., Akhtar, K., Eds.; ItechOpen: London, UK, 2019.
48. Hojamberdiev, M.; Czech, B.; Göktaş, A.C.; Yubuta, K.; Kadirova, Z.C. SnO_2@ZnS Photocatalyst with Enhanced Photocatalytic Activity for the Degradation of Selected Pharmaceuticals and Personal Care Products in Model Wastewater. *J. Alloys Compd.* **2020**, *827*, 154339. [CrossRef]
49. Ahmadpour, N.; Sayadi, M.H.; Sobhani, S.; Hajiani, M. Photocatalytic Degradation of Model Pharmaceutical Pollutant by Novel Magnetic TiO_2@$ZnFe_2O_4$/Pd Nanocomposite with Enhanced Photocatalytic Activity and Stability under Solar Light Irradiation. *J. Environ. Manag.* **2020**, *271*, 110964. [CrossRef]
50. Zhang, Q.; Peng, Y.; Deng, F.; Wang, M.; Chen, D. Porous Z-Scheme MnO_2/Mn-Modified Alkalinized g-C3N4 Heterojunction with Excellent Fenton-like Photocatalytic Activity for Efficient Degradation of Pharmaceutical Pollutants. *Sep. Purif. Technol.* **2020**, *246*, 116890. [CrossRef]
51. Jouyandeh, M.; Tavakoli, O.; Sarkhanpour, R.; Sajadi, S.M.; Zarrintaj, P.; Rabiee, N.; Akhavan, O.; Lima, E.C.; Saeb, M.R. Green Products from Herbal Medicine Wastes by Subcritical Water Treatment. *J. Hazard. Mater.* **2022**, *424*, 127294. [CrossRef]
52. Cregg, R.; Russo, G.; Gubbay, A.; Branford, R.; Sato, H. Pharmacogenetics of Analgesic Drugs. *Br. J. Pain* **2013**, *7*, 2049463713507439. [CrossRef] [PubMed]
53. van Rensburg, R.; Reuter, H. An Overview of Analgesics: Nsaids, Paracetamol, and Topical Analgesics Part 1. *S. Afr. Fam. Pract.* **2019**, *61*, S4–S10. [CrossRef]

54. Wu, S.; Zhang, L.; Chen, J. Paracetamol in the Environment and Its Degradation by Microorganisms. *Appl. Microbiol. Biotechnol.* **2012**, *96*, 875–884. [CrossRef] [PubMed]
55. Acetaminophen (Tylenol): A Pain to the Environment! CHEM 331: Environmental Organic Chemistry March 20, 2008. Available online: https://web.viu.ca/krogh/chem331/Acetaminophen.pdf (accessed on 12 May 2022).
56. Dalida, M.L.P.; Amer, K.M.S.; Su, C.C.; Lu, M.C. Photocatalytic Degradation of Acetaminophen in Modified TiO_2 under Visible Irradiation. *Environ. Sci. Pollut. Res.* **2014**, *21*, 1208–1216. [CrossRef] [PubMed]
57. Lozano-Morales, S.A.; Morales, G.; López Zavala, M.Á.; Arce-Sarria, A.; Machuca-Martínez, F. Photocatalytic Treatment of Paracetamol Using TiO_2 Nanotubes: Effect of PH. *Processes* **2019**, *7*, 319. [CrossRef]
58. Jayasree, P.; Remya, N. Photocatalytic Degradation of Paracetamol Using Aluminosilicate Supported TiO_2. *Water Sci. Technol.* **2020**, *82*, 2114–2124. [CrossRef]
59. Chang, C.T.; Wang, J.J.; Ouyang, T.; Zhang, Q.; Jing, Y.H. Photocatalytic Degradation of Acetaminophen in Aqueous Solutions by TiO_2/ZSM-5 Zeolite with Low Energy Irradiation. *Mater. Sci. Eng. Solid State Mater. Adv. Technol.* **2015**, *196*, 53–60. [CrossRef]
60. Jallouli, N.; Elghniji, K.; Trabelsi, H.; Ksibi, M. Photocatalytic Degradation of Paracetamol on TiO_2 Nanoparticles and TiO_2/Cellulosic Fiber under UV and Sunlight Irradiation. *Arab. J. Chem.* **2017**, *10*, S3640–S3645. [CrossRef]
61. Fernandes, T.A.; Mendo, S.G.; Ferreira, L.P.; Neng, N.R.; Oliveira, M.C.; Gil, A.; Carvalho, M.D.; Monteiro, O.C.; Nogueira, J.M.F.; Calhorda, M.J. Photocatalytic Degradation of Acetaminophen and Caffeine Using Magnetite–Hematite Combined Nanoparticles: Kinetics and Mechanisms. *Environ. Sci. Pollut. Res.* **2021**, *28*, 17228–17243. [CrossRef]
62. Al Marzouqi, F.; Selvaraj, R.; Kim, Y. Rapid Photocatalytic Degradation of Acetaminophen and Levofloxacin Using G-C3N4 Nanosheets under Solar Light Irradiation. *Mater. Res. Express* **2019**, *6*, 125538. [CrossRef]
63. Fan, G.; Peng, H.; Zhang, J.; Zheng, X.; Zhu, G.; Wang, S.; Hong, L. Degradation of Acetaminophen in Aqueous Solution under Visible Light Irradiation by Bi-Modified Titanate Nanomaterials: Morphology Effect, Kinetics and Mechanism. *Catal. Sci. Technol.* **2018**, *8*, 5906–5919. [CrossRef]
64. Sharma, K.; Kaushik, G. NSAIDS in the Environment: From Emerging Problem to Green Solution OPEN ACCESS. *Ann. Pharmacol. Pharm.* **2017**, *2*, 1077.
65. Tyumina, E.A.; Bazhutin, G.A.; Cartagena Gómez, A.D.P.; Ivshina, I.B. Nonsteroidal Anti-Inflammatory Drugs as Emerging Contaminants. *Microbiol. Russian Fed.* **2020**, *89*, 148–163. [CrossRef]
66. Karimi, P.; Baneshi, M.M.; Malakootian, M. Photocatalytic Degradation of Aspirin from Aqueous Solutions Using the UV/ZnO Process: Modelling, Analysis and Optimization by Response Surface Methodology (RSM). *Desalin. Water Treat.* **2019**, *161*, 354–364. [CrossRef]
67. Mukherjee, D.; Ray, A.K.; Barghi, S. Mechanism of Acetyl Salicylic Acid (Aspirin) Degradation under Solar Light in Presence of a TiO_2-Polymeric Film Photocatalyst. *Processes* **2016**, *4*, 13. [CrossRef]
68. Bianchi, C.L.; Sacchi, B.; Pirola, C.; Demartin, F.; Cerrato, G.; Morandi, S.; Capucci, V. Aspirin and Paracetamol Removal Using a Commercial Micro-Sized TiO_2 Catalyst in Deionized and Tap Water. *Environ. Sci. Pollut. Res.* **2017**, *24*, 12646–12654. [CrossRef] [PubMed]
69. Li, L.; Ma, Q.; Wang, S.; Song, S.; Li, B.; Guo, R.; Cheng, X.; Cheng, Q. Photocatalytic Performance and Degradation Mechanism of Aspirin by TiO_2 through Response Surface Methodology. *Catalysts* **2018**, *8*, 118. [CrossRef]
70. Moore, N.; Carleton, B.; Blin, P.; Bosco-Levy, P.; Droz, C. Does Ibuprofen Worsen COVID-19? *Drug Saf.* **2020**, *43*, 611–614. [CrossRef]
71. Tadjarodi, A.; Akhavan, O.; Bijanzad, K.; Khiavi, M.M. Mechanochemically Prepared BiOCl Nanoplates for Removal of Rhodamine B and Pentachlorophenol. *Monatshefte Chemie* **2016**, *147*, 685–696. [CrossRef]
72. Arthur, R.B.; Bonin, J.L.; Ardill, L.P.; Rourk, E.J.; Patterson, H.H.; Stemmler, E.A. Photocatalytic Degradation of Ibuprofen over BiOCl Nanosheets with Identification of Intermediates. *J. Hazard. Mater.* **2018**, *358*, 1–9. [CrossRef]
73. Liu, Y.; Hu, Z.; Yu, J.C. Photocatalytic Degradation of Ibuprofen on S-Doped BiOBr. *Chemosphere* **2021**, *278*, 130376. [CrossRef] [PubMed]
74. Suarez-Escobar, A.F.; Conde-Rivera, L.R.; Lopez-Suarez, F.E.; Illán-Gómez, M.J.; Gonzalez-Hernandez, K.S.; Chalapud-Morales, J.S. Heterogeneous Photocatalytic Degradation of Ibuprofen Over TiO_2–Ag Supported on Activated Carbon from Waste Tire Rubber. *Top. Catal.* **2021**, *64*, 51–64. [CrossRef]
75. Romeiro, A.; Azenha, M.E.; Canle, M.; Rodrigues, V.H.N.; Da Silva, J.P.; Burrows, H.D. Titanium Dioxide Nanoparticle Photocatalysed Degradation of Ibuprofen and Naproxen in Water: Competing Hydroxyl Radical Attack and Oxidative Decarboxylation by Semiconductor Holes. *ChemistrySelect* **2018**, *3*, 10915–10924. [CrossRef]
76. Pelosato, R.; Carrara, V.; Sora, I.N. Enhanced Photocatalytic Degradation of Ibuprofen in Aqueous Solution under Visible-Light Irradiation: Effects of $LaFeO_3$ and Cu/$LaFeO_3$. *Chem. Eng. Trans.* **2019**, *73*, 181–186. [CrossRef]
77. Jallouli, N.; Pastrana-Martínez, L.M.; Ribeiro, A.R.; Moreira, N.F.F.; Faria, J.L.; Hentati, O.; Silva, A.M.T.; Ksibi, M. Heterogeneous Photocatalytic Degradation of Ibuprofen in Ultrapure Water, Municipal and Pharmaceutical Industry Wastewaters Using a TiO_2/UV-LED System. *Chem. Eng. J.* **2018**, *334*, 976–984. [CrossRef]
78. Tanveer, M.; Guyer, G.T.; Abbas, G. Photocatalytic Degradation of Ibuprofen in Water Using TiO_2 and ZnO under Artificial UV and Solar Irradiation. *Water Environ. Res.* **2019**, *91*, 822–829. [CrossRef]
79. Shafeei, N.; Asadollahfardi, G.; Moussavi, G.; Akbar Boojar, M.M. Degradation of Ibuprofen in the Photocatalytic Process with Doped TiO_2 as Catalyst and UVA-LED as Existing Source. *Desalin. Water Treat.* **2019**, *142*, 341–352. [CrossRef]

80. Rastkari, N.; Eslami, A.; Nasseri, S.; Piroti, E.; Asadi, A. Optimizing Parameters on Nanophotocatalytic Degradation of Ibuprofen Using UVC/ZnO Processes by Response Surface Methodology. *Polish J. Environ. Stud.* **2017**, *26*, 785–794. [CrossRef]
81. Mohamed, A.; Salama, A.; Nasser, W.S.; Uheida, A. Photodegradation of Ibuprofen, Cetirizine, and Naproxen by PAN-MWCNT/TiO_2–NH2 Nanofiber Membrane under UV Light Irradiation. *Environ. Sci. Eur.* **2018**, *30*, 1–9. [CrossRef]
82. Khalaf, S.; Shoqeir, J.H.; Lelario, F.; Scrano, L.; Bufo, S.A.; Karaman, R. TiO_2 and Active Coated Glass Photodegradation of Ibuprofen. *Catalysts* **2020**, *10*, 560. [CrossRef]
83. Jiménez-Salcedo, M.; Monge, M.; Tena, M.T. Photocatalytic Degradation of Ibuprofen in Water Using TiO_2/UV and g-C3N4/Visible Light: Study of Intermediate Degradation Products by Liquid Chromatography Coupled to High-Resolution Mass Spectrometry. *Chemosphere* **2019**, *215*, 605–618. [CrossRef] [PubMed]
84. Simon, L.S. Biologic Effects of Nonsteroidal Anti-Inflammatory Drugs. *Curr. Opin. Rheumatol.* **1997**, *9*, 178–182. [CrossRef] [PubMed]
85. Ong, C.K.S.; Lirk, P.; Tan, C.H.; Seymour, R.A. An Evidence-Based Update on Nonsteroidal Anti-Inflammatory Drugs. *Clin. Med. Res.* **2007**, *5*, 19–34. [CrossRef] [PubMed]
86. Wojcieszyńska, D.; Guzik, U. Naproxen in the Environment: Its Occurrence, Toxicity to Nontarget Organisms and Biodegradation. *Appl. Microbiol. Biotechnol.* **2020**, *104*, 1849–1857. [CrossRef]
87. Štrbac, D.; Aggelopoulos, C.A.; Štrbac, G.; Dimitropoulos, M.; Novaković, M.; Ivetić, T.; Yannopoulos, S.N. Photocatalytic Degradation of Naproxen and Methylene Blue: Comparison between ZnO, TiO_2 and Their Mixture. *Proc. Saf. Environ. Prot.* **2018**, *113*, 174–183. [CrossRef]
88. Li, Z.; Liu, G.; Su, Q.; Lv, C.; Jin, X.; Wen, X. UV-Induced Photodegradation of Naproxen Using a Nano γ-FeOOH Composite: Degradation Kinetics and Photocatalytic Mechanism. *Front. Chem.* **2019**, *7*, 1–12. [CrossRef]
89. Fan, G.; Zhan, J.; Luo, J.; Zhang, J.; Chen, Z.; You, Y. Photocatalytic Degradation of Naproxen by a H_2O_2-Modified Titanate Nanomaterial under Visible Light Irradiation. *Catal. Sci. Technol.* **2019**, *9*, 4614–4628. [CrossRef]
90. Kanakaraju, D.; Motti, C.A.; Glass, B.D.; Oelgemöller, M. Solar Photolysis versus TiO_2-Mediated Solar Photocatalysis: A Kinetic Study of the Degradation of Naproxen and Diclofenac in Various Water Matrices. *Environ. Sci. Pollut. Res.* **2016**, *23*, 17437–17448. [CrossRef]
91. Jallouli, N.; Elghniji, K.; Hentati, O.; Ribeiro, A.R.; Silva, A.M.T.; Ksibi, M. UV and Solar Photo-Degradation of Naproxen: TiO_2 Catalyst Effect, Reaction Kinetics, Products Identification and Toxicity Assessment. *J. Hazard. Mater.* **2016**, *304*, 329–336. [CrossRef]
92. Karimi, P.; Malakootian, M. Optimization of Photocatalytic Degradation of Naproxen from Aqueous Solutions with UV/ZnO Process: Response Surface Methodology (RSM). *Glob. Nest J.* **2020**, *22*, 369–380. [CrossRef]
93. Fan, G.; Ning, R.; Luo, J.; Zhang, J.; Hua, P.; Guo, Y.; Li, Z. Visible-Light-Driven Photocatalytic Degradation of Naproxen by Bi-Modified Titanate Nanobulks: Synthesis, Degradation Pathway and Mechanism. *J. Photochem. Photobiol. Chem.* **2020**, *386*, 112108. [CrossRef]
94. Fu, K.; Pan, Y.; Ding, C.; Shi, J.; Deng, H. Reduced Graphene Oxide/ZnIn2S4 Nanocomposite Photocatalyst with Enhanced Photocatalytic Performance for the Degradation of Naproxen under Visible Light Irradiation. *Catalysts* **2020**, *10*, 710. [CrossRef]
95. Gupta, R.; Wadhwa, R. *Mucolytic Medications*; StatPearls Publishing: Treasure Island, FL, USA, 2021.
96. Wilkinson, M.; Sugumar, K.; Milan, S.J.; Hart, A.; Crockett, A.; Crossingham, I. Mucolytics for Bronchiectasis. *Cochrane Database Syst. Rev.* **2014**, *2014*, 1289. [CrossRef] [PubMed]
97. Olaleye, O.A.; Kaur, M.; Onyenaka, C.C. Ambroxol Hydrochloride Inhibits the Interaction between Severe Acute Respiratory Syndrome Coronavirus 2 Spike Protein's Receptor Binding Domain and Recombinant Human ACE2. *bioRxiv Prepr. Serv. Biol.* **2020**. [CrossRef]
98. Tab, A.; Dahmane, M.; Belabed, C.; Bellal, B.; Richard, C.; Trari, M. High Efficiency Photocatalytic Degradation of Ambroxol over Mn Doped TiO_2: Experimental Designs, Identification of Transformation Products, Mineralization and Mechanism. *Sci. Total Environ.* **2021**, *780*, 146451. [CrossRef]
99. Bielen, A.; Šimatović, A.; Kosić-Vukšić, J.; Senta, I.; Ahel, M.; Babić, S.; Jurina, T.; González Plaza, J.J.; Milaković, M.; Udiković-Kolić, N. Negative Environmental Impacts of Antibiotic-Contaminated Effluents from Pharmaceutical Industries. *Water Res.* **2017**, *126*, 79–87. [CrossRef]
100. Polianciuc, S.I.; Gurzău, A.E.; Kiss, B.; Georgia Ștefan, M.; Loghin, F. Antibiotics in the Environment: Causes and Consequences. *Med. Pharm. Rep.* **2020**, *93*, 231. [CrossRef]
101. Čizmić, M.; Ljubas, D.; Rožman, M.; Ašperger, D.; Ćurković, L.; Babíc, S. Photocatalytic Degradation of Azithromycin by Nanostructured TiO_2 Film: Kinetics, Degradation Products, and Toxicity. *Materials* **2019**, *16*, 873. [CrossRef]
102. Luo, X.; Hao, T.; Yue, L.; Hong, G.; Lu, Y. *Azithromycin Wastewater Treatment with La Doping Titanium Dioxide /Active Carbon Composites*; Atlantis Press: Amsterdam, The Netherlands, 2016; pp. 861–870. [CrossRef]
103. Akhavan, O.; Ghaderi, E. Photocatalytic Reduction of Graphene Oxide Nanosheets on TiO_2 Thin Film for Photoinactivation of Bacteria in Solar Light Irradiation. *J. Phys. Chem.* **2009**, *113*, 20214–20220. [CrossRef]
104. Naraginti, S.; Yu, Y.Y.; Fang, Z.; Yong, Y.C. Visible Light Degradation of Macrolide Antibiotic Azithromycin by Novel ZrO_2/Ag@TiO_2 Nanorod Composite: Transformation Pathways and Toxicity Evaluation. *Proc. Saf. Environ. Prot.* **2019**, *125*, 39–49. [CrossRef]
105. Ospino-Atehortúa, B.A.; Zúñiga-Benítez, H.; Peñuela, G.A. Potential Application of Persulfate and Simulated Sunlight Radiation on Azithromycin Removal. *Environ. Eng. Res.* **2021**, *26*, 200189. [CrossRef]

106. Li, C.; Jin, H.; Hou, Z.; Guo, Y. Study on Degradation of Azithromycin Antibiotics by Molybdenum Sulfide Graphene Oxide Composites under Visible Light. *IOP Conf. Ser. Mater. Sci. Eng.* **2020**, *774*, 012019. [CrossRef]
107. Sayadi, M.H.; Sobhani, S.; Shekari, H. Photocatalytic Degradation of Azithromycin Using GO@Fe_3O_4/ ZnO/ SnO_2 Nanocomposites. *J. Clean. Prod.* **2019**, *232*, 127–136. [CrossRef]
108. Pham, T.D.M.; Ziora, Z.M.; Blaskovich, M.A.T. Quinolone Antibiotics. *Medchemcomm* **2019**, *10*, 1719–1739. [CrossRef]
109. Sirtori, C.; Zapata, A.; Malato, S.; Gernjak, W.; Fernández-Alba, A.R.; Agüera, A. Solar Photocatalytic Treatment of Quinolones: Intermediates and Toxicity Evaluation. *Photochem. Photobiol. Sci.* **2009**, *8*, 644–651. [CrossRef]
110. Song, W.; Muste, J.C.; Greenlee, T.E.; Singh, R.P. Chloroquine and Hydroxychloroquine Toxicity. *Am. J. Ophthalm. Clin. Trials* **2020**, *129*, 1506–1507. [CrossRef]
111. Gasmi, A.; Peana, M.; Noor, S.; Lysiuk, R.; Menzel, A.; Gasmi Benahmed, A.; Bjørklund, G. Chloroquine and Hydroxychloroquine in the Treatment of COVID-19: The Never-Ending Story. *Appl. Microbiol. Biotechnol.* **2021**, *105*, 1333–1343. [CrossRef]
112. da Silva, P.L.; Nippes, R.P.; Macruz, P.D.; Hegeto, F.L.; Olsen Scaliante, M.H.N. Photocatalytic Degradation of Hydroxychloroquine Using ZnO Supported on Clinoptilolite Zeolite. *Water Sci. Technol.* **2021**, *84*, 763–776. [CrossRef]
113. Bensalah, N.; Midassi, S.; Ahmad, M.I.; Bedoui, A. Degradation of Hydroxychloroquine by Electrochemical Advanced Oxidation Processes. *Chem. Eng. J.* **2020**, *402*, 126279. [CrossRef]
114. Yi, X.H.; Ji, H.; Wang, C.C.; Li, Y.; Li, Y.H.; Zhao, C.; Wang, A.; Fu, H.; Wang, P.; Zhao, X.; et al. Photocatalysis-Activated SR-AOP over PDINH/MIL-88A(Fe) Composites for Boosted Chloroquine Phosphate Degradation: Performance, Mechanism, Pathway and DFT Calculations. *Appl. Catal. Environ.* **2021**, *293*, 120229. [CrossRef]
115. Barnes, P.J. Anti-Inflammatory Actions of Glucocorticoids: Molecular Mechanisms. *Clin. Sci.* **1998**, *94*, 557–572. [CrossRef]
116. Dexamethasone in Hospitalized Patients with Covid-19. *N. Engl. J. Med.* **2021**. [CrossRef]
117. Vardy, J.; Chiew, K.S.; Galica, J.; Pond, G.R.; Tannock, I.F. Side Effects Associated with the Use of Dexamethasone for Prophylaxis of Delayed Emesis after Moderately Emetogenic Chemotherapy. *Br. J. Cancer* **2006**, *94*, 1011–1015. [CrossRef]
118. Pazoki, M.; Parsa, M.; Farhadpour, R. Removal of the Hormones Dexamethasone (DXM) by Ag Doped on TiO_2 Photocatalysis. *J. Environ. Chem. Eng.* **2016**, *4*, 4426–4434. [CrossRef]
119. Ghenaatgar, A.; Tehrani, R.M.A.; Khadir, A. Photocatalytic Degradation and Mineralization of Dexamethasone Using WO_3 and ZrO_2 Nanoparticles: Optimization of Operational Parameters and Kinetic Studies. *J. Water Process Eng.* **2019**, *32*, 100969. [CrossRef]
120. da Silva, W.L.; Lansarin, M.A.; dos Santos, J.H.Z.; Da Rocha, Z.N.; Pepe, I.M. Electrochemical and Catalytic Studies of a Supported Photocatalyst Produced from Petrochemical Residue in the Photocatalytic Degradation of Dexamethasone and Guaifenesin Drugs. *Water. Air. Soil Pollut.* **2016**, *227*, 1–9. [CrossRef]
121. Awwad, N.S.; El-Khalafawy, A.; Ibrahium, H.A.; Hamdy, M.S. Photocatalytic Degradation of Cortisone Acetate by Using Graphite Doped Ceria Nanoparticles under Visible Light Illumination. *Mater. Res. Express* **2019**, *6*, 095907. [CrossRef]
122. Amani, H.; Habibey, R.; Hajmiresmail, S.J.; Latifi, S.; Pazoki-Toroudi, H.; Akhavan, O. Antioxidant Nanomaterials in Advanced Diagnoses and Treatments of Ischemia Reperfusion Injuries. *J. Mater. Chem.* **2017**, *5*, 9452–9476. [CrossRef] [PubMed]
123. Amani, H.; Habibey, R.; Shokri, F.; Hajmiresmail, S.J.; Akhavan, O.; Mashaghi, A.; Pazoki-Toroudi, H. Selenium Nanoparticles for Targeted Stroke Therapy through Modulation of Inflammatory and Metabolic Signaling. *Sci. Rep.* **2019**, *9*, 1–15. [CrossRef]
124. Kosonen, J.; Kronberg, L. The Occurrence of Antihistamines in Sewage Waters and in Recipient Rivers. *Environ. Sci. Pollut. Res.* **2009**, *16*, 555–564. [CrossRef]
125. Abdel-Raouf, N.; Al-Homaidan, A.A.; Ibraheem, I.B.M. Microalgae and Wastewater Treatment. *Saudi J. Biol. Sci.* **2012**, *19*, 257–275. [CrossRef] [PubMed]
126. Gelotte, C.K.; Zimmerman, B.A.; Thompson, G.A. Single-Dose Pharmacokinetic Study of Diphenhydramine HCl in Children and Adolescents. *Clin. Pharmacol. Drug Dev.* **2018**, *7*, 400–407. [CrossRef] [PubMed]
127. Song, L.; Yi, C.; Wu, Q.; Li, Z.; Zhang, W.; Hong, H. Photocatalytic Degradation of Diphenhydramine in Aqueous Solution by Natural Dolomite. *RSC Adv.* **2020**, *10*, 38663–38671. [CrossRef] [PubMed]
128. Pastrana-Martínez, L.M.; Faria, J.L.; Doña-Rodríguez, J.M.; Fernández-Rodríguez, C.; Silva, A.M.T. Degradation of Diphenhydramine Pharmaceutical in Aqueous Solutions by Using Two Highly Active TiO_2 Photocatalysts: Operating Parameters and Photocatalytic Mechanism. *Appl. Catal. Environ.* **2012**, *113–114*, 221–227. [CrossRef]
129. López, N.; Marco, P.; Giménez, J.; Esplugas, S. Photocatalytic Diphenhydramine Degradation under Different Radiation Sources: Kinetic Studies and Energetic Comparison. *Appl. Catal. Environ.* **2018**, *220*, 497–505. [CrossRef]
130. Morales-Torres, S.; Pastrana-Martínez, L.M.; Figueiredo, J.L.; Faria, J.L.; Silva, A.M.T. Graphene Oxide-P25 Photocatalysts for Degradation of Diphenhydramine Pharmaceutical and Methyl Orange Dye. *Appl. Surf. Sci.* **2013**, *275*, 361–368. [CrossRef]
131. Davari, N.; Farhadian, M.; Nazar, A.R.S.; Homayoonfal, M. Degradation of Diphenhydramine by the Photocatalysts of ZnO/Fe_2O_3 and TiO_2/Fe_2O_3 Based on Clinoptilolite: Structural and Operational Comparison. *J. Environ. Chem. Eng.* **2017**, *5*, 5707–5720. [CrossRef]
132. Arai, N.; Nakamizo, T.; Ihara, H.; Koide, T.; Nakamura, A.; Tabuse, M.; Miyazaki, H. Histamine H2-Blocker and Proton Pump Inhibitor Use and the Risk of Pneumonia in Acute Stroke: A Retrospective Analysis on Susceptible Patients. *PLoS ONE* **2017**, *12*, e0169300. [CrossRef]

133. Vatti, S.K.; Gupta, S.; Raj, R.P.; Selvam, P. Periodic Mesoporous Titania with Anatase and Bronze Phases—The New Generation Photocatalyst: Synthesis, Characterisation, and Application in Environmental Remediation. *New J. Chem.* **2020**, *44*, 16269–16284. [CrossRef]
134. Molla, M.A.I.; Tateishi, I.; Furukawa, M.; Katsumata, H.; Suzuki, T.; Kaneco, S. Photocatalytic Removal of Famotidine with TiO_2 from Water in the Presence of Dye under Visible Light Irradiation. *Desalin. Water Treat.* **2017**, *87*, 338–347. [CrossRef]
135. Keane, D.; Basha, S.; Nolan, K.; Morrissey, A.; Oelgemöller, M.; Tobin, J.M. Photodegradation of Famotidine by Integrated Photocatalytic Adsorbent (IPCA) and Kinetic Study. *Catal. Lett.* **2011**, *141*, 300–308. [CrossRef]
136. Abongwa, M.; Martin, R.J.; Robertson, A.P. A Brief Review on the Mode of Action of Antinematodal Drugs. *Acta Vet. Brno.* **2017**, *67*, 137–152. [CrossRef] [PubMed]
137. Chalfie, M.; Girard, L. WormBook the Online Review of C. Elegans Biology. *West Coast Worm Meet.* **2007**, *35*, D472–D475.
138. Chai, J.Y. Praziquantel Treatment in Trematode and Cestode Infections: An Update. *Infect. Chemother.* **2013**, *45*, 32–43. [CrossRef]
139. Oyeyemi, O.T.; Okunlola, O.A.; Adebayo, A.D. Assessment of Schistosomiasis Endemicity and Preventive Treatment on Coronavirus Disease 2019 Outcomes in Africa. *New Microb. New Infect.* **2020**, *38*, 100821. [CrossRef]
140. Čizmić, M.; Ljubas, D.; Ćurković, L.; Škorić, I.; Babić, S. Kinetics and Degradation Pathways of Photolytic and Photocatalytic Oxidation of the Anthelmintic Drug Praziquantel. *J. Hazard. Mater.* **2017**, *323*, 500–512. [CrossRef]
141. Rossignol, J.F. Nitazoxanide: A First-in-Class Broad-Spectrum Antiviral Agent. *Antiv. Res.* **2014**, *110*, 94–103. [CrossRef]
142. Bryant, A.; Lawrie, T.A.; Dowswell, T.; Fordham, E.J.; Mitchell, S.; Hill, S.R.; Tham, T.C. Ivermectin for Prevention and Treatment of COVID-19 Infection: A Systematic Review, Meta-Analysis, and Trial Sequential Analysis to Inform Clinical Guidelines. *Am. J. Ther.* **2021**, *28*, e434–e460. [CrossRef]
143. Havlíková, L.; Šatínský, D.; Solich, P. Aspects of Decontamination of Ivermectin and Praziquantel from Environmental Waters Using Advanced Oxidation Technology. *Chemosphere* **2016**, *144*, 21–28. [CrossRef]
144. Bosco, S.M.D.; Barbosa, I.M.; Candello, F.P.; Maniero, M.G.; Rath, S.; Guimaraes, J.R. Degradation of Ivermectin by Fenton and Photo-Fenton and Toxicity Test Using Daphnia Similis. *J. Adv. Oxid. Technol.* **2011**. [CrossRef]
145. Rafailidis, P.I.; Mavros, M.N.; Kapaskelis, A.; Falagas, M.E. Antiviral Treatment for Severe EBV Infections in Apparently Immunocompetent Patients. *J. Clin. Virol.* **2010**, *49*, 151–157. [CrossRef] [PubMed]
146. Wagstaff, A.J.; Faulds, D.; Goa, K.L. Aciclovir: A Reappraisal of Its Antiviral Activity, Pharmacokinetic Properties and Therapeutic Efficacy. *Drugs* **1994**, *47*, 153–205. [CrossRef] [PubMed]
147. Russo, D.; Siciliano, A.; Guida, M.; Galdiero, E.; Amoresano, A.; Andreozzi, R.; Reis, N.M.; Li Puma, G.; Marotta, R. Photodegradation and Ecotoxicology of Acyclovir in Water under UV254 and UV254/H2O2 Processes. *Water Res.* **2017**, *122*, 591–602. [CrossRef]
148. An, T.; An, J.; Gao, Y.; Li, G.; Fang, H.; Song, W. Photocatalytic Degradation and Mineralization Mechanism and Toxicity Assessment of Antivirus Drug Acyclovir: Experimental and Theoretical Studies. *Appl. Catal. Environ.* **2015**, *164*, 279–287. [CrossRef]
149. Zhou, C.; Chen, J.; Xie, Q.; Wei, X.; Zhang, Y.N.; Fu, Z. Photolysis of Three Antiviral Drugs Acyclovir, Zidovudine and Lamivudine in Surface Freshwater and Seawater. *Chemosphere* **2015**, *138*, 792–797. [CrossRef] [PubMed]
150. Jia, T.C.; Guo, J.T.; Wang, Z.; Zhu, X.S.; Zhang, Q.X.; Chen, P.; Yao, K.; Lv, W.Y.; Liu, G.G. Photodegradation Mechanisms of Acyclovir in Water and the Toxicity of Photoproducts. *J. Radioanal. Nucl. Chem.* **2019**, *320*, 823–830. [CrossRef]
151. Alhumaid, S.; Al Mutair, A.; Al Alawi, Z.; Alhmeed, N.; Zaidi, A.R.Z.; Tobaiqy, M. Efficacy and Safety of Lopinavir/Ritonavir for Treatment of COVID-19: A Systematic Review and Meta-Analysis. *Trop. Med. Infect. Dis.* **2020**, *5*, 180. [CrossRef]
152. Horby, P.W.; Mafham, M.; Bell, J.L.; Linsell, L.; Staplin, N.; Emberson, J.; Palfreeman, A.; Raw, J.; Elmahi, E.; Prudon, B.; et al. Lopinavir–Ritonavir in Patients Admitted to Hospital with COVID-19 (RECOVERY): A Randomised, Controlled, Open-Label, Platform Trial. *Lancet* **2020**, *396*, 1345–1352. [CrossRef]
153. Bhavyasri, K.; Murali Balaram, V.; Nageswarao, R.; Rambabu, D.; Sasikiran Goud, E.; Ajitha, M. Development and Validation of Forced Degradation Studies of Atazanavir Using RP-HPLC and Characterization of Degradants by LC-MS/MS. *Int. J. Pharm. Sci. Rev. Res.* **2015**, *33*, 11–15.
154. Donato, E.M.; Dias, C.L.; Rossi, R.C.; Valente, R.S.; Fröehlich, P.E.; Bergold, A.M. LC Method for Studies on the Stability of Lopinavir and Ritonavir in Soft Gelatin Capsules. *Chromatographia* **2006**, *63*, 437–443. [CrossRef]
155. Agrawal, U.; Raju, R.; Udwadia, Z.F. Favipiravir: A New and Emerging Antiviral Option in COVID-19. *Med. J. Armed Forces India* **2020**. [CrossRef] [PubMed]
156. Nakayama, T.; Honda, R. Electrochemical and Mechanistic Study of Oxidative Degradation of Favipiravir by Electrogenerated Superoxide through Proton-Coupled Electron Transfer. *ACS Omega* **2021**, *6*, 21730–21740. [CrossRef] [PubMed]
157. Di Santo, N.; Ehrisman, J. Research Perspective: Potential Role of Nitazoxanide in Ovarian Cancer Treatment. Old Drug, New Purpose? *Cancers* **2013**, *5*, 1163–1176. [CrossRef] [PubMed]
158. White, A.C. Nitazoxanide: A New Broad Spectrum Antiparasitic Agent. *Expert Rev. Anti. Infect. Ther.* **2004**, *2*, 43–49. [CrossRef]
159. Zerón, H.M.; Calderón, J.M.; Coria, L.P.; Figueroa, J.M.; Vargas Contreras, M.J.; Aceves, H.L.V.; Salazar, F.M.C.; Hernández, D.C.; Vidaurri, E.M.; González, A.C.; et al. Nitazoxanide as an Early Treatment to Reduce the Intensity of COVID-19 Outbreaks among Health Personnel. *World Acad. Sci. J.* **2021**, *3*, 1–6. [CrossRef]
160. Malesuik, M.D.; Gonçalves, H.M.L.; Paim, C.S.; Schapoval, E.E.S.; Steppe, M. LC: Analysis of Photodegradation Kinetics of Nitazoxanide in Pharmaceutical Formulations. *J. Chromatogr. Sci.* **2009**, *47*, 745–748. [CrossRef]

161. Kokic, G.; Hillen, H.S.; Tegunov, D.; Dienemann, C.; Seitz, F.; Schmitzova, J.; Farnung, L.; Siewert, A.; Höbartner, C.; Cramer, P. Mechanism of SARS-CoV-2 Polymerase Stalling by Remdesivir. *Nat. Commun.* **2021**, *12*, 1–7. [CrossRef]
162. Beigel, J.H.; Tomashek, K.M.; Dodd, L.E.; Mehta, A.K.; Zingman, B.S.; Kalil, A.C.; Hohmann, E.; Chu, H.Y.; Luetkemeyer, A.; Kline, S.; et al. Remdesivir for the Treatment of Covid-19—Final Report. *N. Engl. J. Med.* **2020**, *383*, 1813–1826. [CrossRef]
163. Hamdy, M.M.A.; Abdel Moneim, M.M.; Kamal, M.F. Accelerated Stability Study of the Ester Prodrug Remdesivir: Recently FDA-Approved Covid-19 Antiviral Using Reversed-Phase-HPLC with Fluorimetric and Diode Array Detection. *Biomed. Chromatogr.* **2021**, *35*, e5212. [CrossRef] [PubMed]
164. Vartak, R.; Patil, S.M.; Saraswat, A.; Patki, M.; Kunda, N.K.; Patel, K. Aerosolized Nanoliposomal Carrier of Remdesivir: An Effective Alternative for COVID-19 Treatment in Vitro. *Nanomedicine* **2021**, *16*, 1187–1202. [CrossRef]